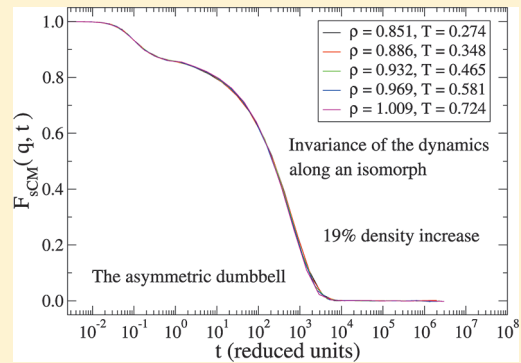


# Isomorphs in Model Molecular Liquids

Trond S. Ingebrigtsen,\* Thomas B. Schrøder, and Jeppe C. Dyre

DNRF Centre “Glass and Time”, IMFUFA, Department of Sciences, Roskilde University, Postbox 260, DK-4000 Roskilde, Denmark

**ABSTRACT:** Isomorphs are curves in the phase diagram along which a number of static and dynamic quantities are invariant in reduced units (Gnan, N.; et al. *J. Chem. Phys.* 2009, 131, 234504). A liquid has good isomorphs if and only if it is strongly correlating, i.e., if the equilibrium virial/potential energy fluctuations are more than 90% correlated in the *NVT* ensemble. Isomorphs were previously discussed with a focus on atomic systems. This paper generalizes isomorphs to liquids composed of rigid molecules and study the isomorphs of systems of small rigid molecules: the asymmetric dumbbell model, a symmetric inverse power-law dumbbell, and the Lewis–Wahnström *o*-terphenyl (OTP) model. For all model systems, the following quantities are found to be invariant along an isomorph: the isochoric heat capacity, the excess entropy, the reduced molecular center-of-mass self-part of the intermediate scattering function, and the reduced molecular center-of-mass radial distribution function. In agreement with theory, we also find that an instantaneous change of temperature and density from an equilibrated state point to an isomorphic state point leads to no relaxation. The isomorphs of the Lewis–Wahnström OTP model were found to be more approximative than those of the asymmetric dumbbell model; this is consistent with the OTP model being less strongly correlating. The asymmetric dumbbell and Lewis–Wahnström OTP models each have a “master isomorph”; i.e., the isomorphs have identical shape in the virial/potential energy phase diagram.



## I. INTRODUCTION

For supercooled liquids near the glass transition changing slightly the density  $\rho$  or temperature  $T$  the structural relaxation time  $\tau_\alpha$  may change several orders of magnitude. In the study of these liquids<sup>1–3</sup> it is often found that  $\tau_\alpha$  does not change when  $\rho^\gamma/T$  is kept constant, where  $\gamma$  is a material-specific exponent. This phenomenon is called *density scaling* (or *thermodynamic scaling*) and has been established for many liquids, excluding associative liquids such as water.<sup>3</sup> A related observation is *isochronal superposition*,<sup>3–5</sup> i.e., that supercooled state points with identical  $\tau_\alpha$  have the same dielectric spectrum. A different and at first sight unrelated concept is Rosenfeld's *excess entropy scaling*.<sup>6,7</sup> In this procedure a relation is established between hard-to-predict dynamic properties and easier-to-predict thermodynamic quantities, here the excess entropy, via a scaling of the dynamics to so-called reduced units. Initially, this was observed for model atomic liquids,<sup>6,7</sup> but later it was extended to model molecular liquids<sup>8–10</sup> and experimental liquids.<sup>11–14</sup> The importance of using reduced units with regards to density scaling of experimental data has recently been pointed out.<sup>15,16</sup>

In a recent series of papers<sup>17–21</sup> a new class of liquids was identified. These liquids are characterized by having strong correlation in the *NVT* ensemble between the equilibrium fluctuations of the potential energy  $U$  and the virial  $W$ . Recall that the instantaneous energy  $E$  and pressure  $p$  can be written as a sum of a kinetic part and a configurational part:  $E = K + U$  and  $pV = Nk_B T + W$ , respectively. The correlation between  $U$  and  $W$  is quantified via the linear correlation coefficient

$R$  defined as

$$R = \frac{\langle \Delta W \Delta U \rangle}{\sqrt{\langle (\Delta W)^2 \rangle} \sqrt{\langle (\Delta U)^2 \rangle}} \quad (1)$$

The class of strongly correlating liquids is defined by  $R \geq 0.90$ .<sup>17</sup> An inverse power-law (IPL) system  $r^{-n}$  has correlation coefficient  $R = 1$ , because for all microconfigurations  $W = (n/3)U$ , and only IPL systems are perfectly correlating. In the study of strongly correlating liquids it was discovered that they obey Rosenfeld's excess entropy scaling, isochronal superposition, as well as density scaling.<sup>20–23</sup> These types of scalings can be explained in the framework of so-called isomorphs (definition follows later).

Model systems that have been identified<sup>17,18,22,24–26</sup> to belong to this class of liquids include the standard single-component Lennard-Jones liquid (SCLJ), the Kob–Andersen binary LJ mixture<sup>27,28</sup> (KABLJ), the asymmetric dumbbell model,<sup>22</sup> the Lewis–Wahnström *o*-terphenyl model<sup>29,30</sup> (OTP), and others. Strong  $WU$  correlation has been experimentally verified for a molecular van der Waals liquid<sup>31</sup> and for supercritical argon.<sup>24</sup> The class of strongly correlating liquids includes most or all van der Waals and metallic liquids, whereas covalently, hydrogen-bonding, or ionic liquids are generally not strongly correlating.<sup>17</sup> The latter

**Received:** August 12, 2011

**Revised:** October 25, 2011

**Published:** January 17, 2012

reflects the fact that competing interactions tend to destroy the strong correlation.

An example of strong *WU* correlation is given in Figure 1 for the asymmetric dumbbell model<sup>22</sup> (details of this model are provided in section III). Figure 1a shows the time evolution of the equilibrium fluctuations of *U* and *W* normalized to zero mean and unity standard deviation; Figure 1b shows a scatter plot of the corresponding values of *U* and *W*. *U* and *W* are clearly strongly correlated in their equilibrium fluctuations.

References 17 and 18 identified the cause of strong *WU* correlation in the SCLJ liquid. The LJ pair potential can be well approximated from  $r = 0.95\sigma$  to  $r = 1.5\sigma$  (Pedersen et al.<sup>23</sup>) by a sum of an IPL, a linear term, and a constant via the so-called “extended IPL potential”:  $v_{\text{LJ}}(r) \approx Ar^{-n} + B + Cr$ . At moderate pressures this covers the entire first peak of the radial distribution function, i.e., the first coordination shell. The constraint of constant volume in the *NVT* ensemble has the effect that when one nearest neighbor distance increases, another one decreases; upon summation the contribution from the linear term to *U* and *W* is almost constant. The latter observation has the consequence that some of the scaling properties of pure IPL systems are inherited in the LJ system in the form of isomorphs.

Reference 20 introduced a new concept referring to a strongly correlating atomic liquid's phase diagram, namely isomorphic curves or more briefly: isomorphs. Two state points with density and temperature ( $\rho_1, T_1$ ) and ( $\rho_2, T_2$ ) are defined to be isomorphic<sup>32</sup> if the following holds: Whenever a configuration of state point (1) and one of state point (2) have the same reduced coordinates ( $\rho_1^{1/3}\mathbf{r}_i^{(1)} = \rho_2^{1/3}\mathbf{r}_i^{(2)}$  for all particles *i*), these two configurations have proportional Boltzmann factors, i.e.,

$$e^{-U(\mathbf{r}_1^{(1)}, \dots, \mathbf{r}_N^{(1)})/k_B T_1} = C_{12} e^{-U(\mathbf{r}_1^{(2)}, \dots, \mathbf{r}_N^{(2)})/k_B T_2} \quad (2)$$

Here  $C_{12}$  is a constant that depends only on the state points (1) and (2). An isomorph is defined as a continuous curve of state points that are all pairwise isomorphic. In other words, eq 2 defines an equivalence relation with the equivalence classes being the isomorphs. Only IPL systems have exact isomorphs; these are characterized by having  $\rho^\gamma/T = \text{const}$  where  $\gamma = n/3$ . Reference 20 argued analytically and demonstrated by simulations that strongly correlating atomic liquids have isomorphs to a good approximation.

From the defining property of an isomorph (eq 2) it follows that the structure in reduced units ( $\tilde{\mathbf{r}}_i \equiv \rho^{1/3}\mathbf{r}_i$ ) is invariant along an isomorph, because the proportionality constant  $C_{12}$  disappears when the configurational canonical probabilities are normalized.<sup>20</sup> Thus the reduced unit radial distribution function and the excess entropy  $S_{\text{ex}} = S - S_{\text{id}}$  are isomorph invariants, where  $S_{\text{id}}$  is the ideal gas contribution to the entropy at the same temperature and density. Isomorph invariance is, however, not limited to static quantities; also the mean-square displacement, time autocorrelation functions, and higher-order correlation functions are invariant in reduced units along an isomorph. The reader is referred to ref 20 for a detailed description of isomorph invariants, as well as the proof that a liquid is strongly correlating if and only if it has good isomorphs. A brief overview of strongly correlating liquids and their isomorphs can be found in Pedersen et al.<sup>23</sup>

Reference 21 studied isomorphs of atomic single-component and multi-component LJ liquids with generalized exponents *m* and *n*. It was found that for given exponents (*m, n*) all isomorphs have the same shape in the *WU* phase diagram; i.e., a so-called master isomorph exists from which all isomorphs can be generated

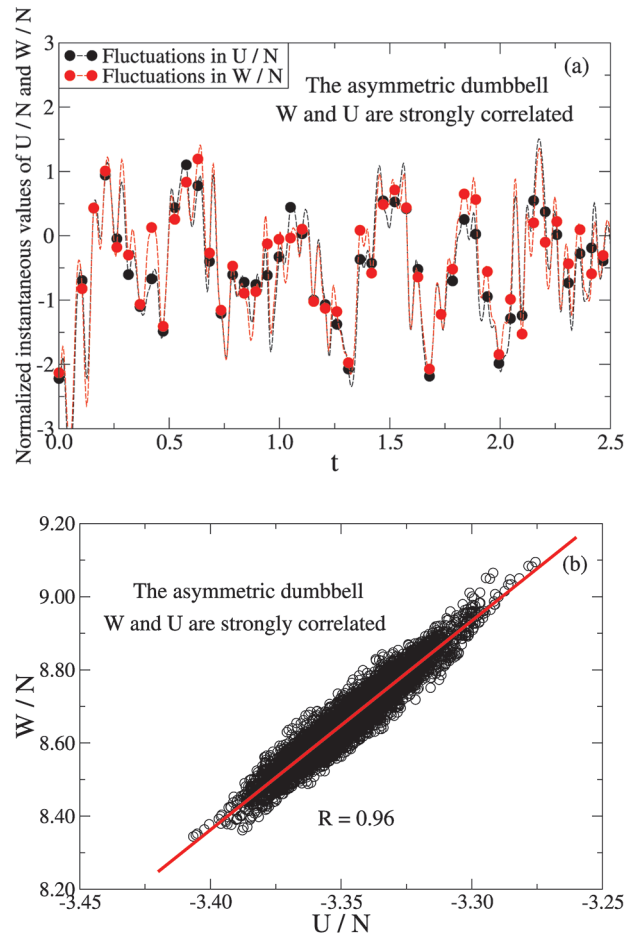


**Figure 1.** Two different ways of visualizing the strong virial/potential energy correlation for the asymmetric dumbbell model at  $\rho = 0.932$  and  $T = 0.465$  (see section III for details of the model and the units used). (a) Time evolution of *U* (black) and *W* (red) per particle normalized to zero mean and unity standard deviation. (b) Scatter plot of the instantaneous values of *W* and *U* per particle. The correlation coefficient *R* is 0.96.

via a simple scaling of the *WU* coordinates. For instance, the shape of isomorphs in the *WU* phase diagram of the SCLJ liquid and the KABLIJ liquid are the same.

References 17–21 focused on understanding strong *WU* correlation and its implication for atomic systems. Schröder et al.<sup>22</sup> in 2008 studied two rigid molecular liquids that are strongly correlating: the asymmetric dumbbell model and the Lewis–Wahnström OTP model (section III). At that time the isomorph concept had not yet been developed, and state points with the same  $\rho^\gamma/T$ , as inspired from the IPL system, were tested for collapse of, for instance, the reduced unit radial distribution function (note that in refs 17, 18, and 22  $\gamma$  is defined slightly different from subsequent papers). The dynamics in reduced units was also found to be a function of  $\rho^\gamma/T$ , to a good approximation, as is the case for IPL systems.<sup>19</sup> Chopra et al.<sup>10</sup> found that the  $S_{\text{ex}}$  can be written (approximately) as a function of  $\rho^\gamma/T$  for rigid symmetric LJ dumbbells with different bond lengths. They also found that the reduced unit diffusion constant and relaxation time are functions of  $S_{\text{ex}}$ . These results suggest that the isomorph concept is relevant also for rigid molecular systems. In this paper we expand on earlier results by studying in detail the same systems as Schröder et al.<sup>22</sup>

The isomorph definition eq 2 must be modified for rigid molecules, because the bond lengths are fixed and cannot follow the overall scaling. A simple modification of eq 2, which is consistent with the atomic definition, is to define the mapping among configurations in terms of the molecular center-of-masses, instead of the atomic positions. We thus define two state points in the phase diagram of a liquid composed of *rigid* molecules to be isomorphic if the following holds: Whenever two configurations of the state points have identical reduced center-of-mass coordinates for all molecules,

$$\rho_1^{1/3} \mathbf{r}_{CM,i}^{(1)} = \rho_2^{1/3} \mathbf{r}_{CM,i}^{(2)} \quad (3)$$

as well as identical Eulerian angles<sup>33</sup>

$$\phi_i^{(1)} = \phi_i^{(2)} \quad \theta_i^{(1)} = \theta_i^{(2)} \quad \chi_i^{(1)} = \chi_i^{(2)} \quad (4)$$

these two configurations have proportional Boltzmann factors, i.e., [where  $\mathbf{R} \equiv (\mathbf{r}_{CM,1}, \phi_1, \theta_1, \chi_1, \dots, \mathbf{r}_{CM,N}, \phi_N, \theta_N, \chi_N)$ ]

$$e^{-U(\mathbf{R}^{(1)})/k_B T_1} = C_{12} e^{-U(\mathbf{R}^{(2)})/k_B T_2} \quad (5)$$

Again,  $C_{12}$  is a constant that depends only on the state points 1 and 2. An isomorph is defined as a set of state points that are pairwise isomorphic. It should be noted that, in contrast to what is the case for atomic systems, because the bonds do not follow the overall scaling of the system, this definition does not imply the existence of exact isomorphs for rigid molecules with IPL interactions between atoms of different molecules.

Taking the logarithm of eq 5 implies

$$U(\mathbf{R}^{(2)}) = T_2/T_1 \cdot U(\mathbf{R}^{(1)}) + k_B T_2 \ln C_{12} \quad (6)$$

Equation 6 provides a convenient way of testing to what extent eq 5 is obeyed for a given system: A simulation is performed at one state point (1) and the obtained configurations are scaled to a different density  $\rho_2$ , where the potential energy is evaluated. The respective potential energies of the two state points are then plotted against each other. In the resulting plot a near straight-line *indicates*, because a liquid is usually not perfectly strongly correlating, that there exists an isomorphic state point with density  $\rho_2$ . The temperature  $T_2$  of the isomorphic state point can be found from the slope of a linear regression fit. This procedure is termed the “direct isomorph check”.<sup>20</sup> If this test is performed for an atomic IPL system, a correlation coefficient of  $R = 1$  is obtained, consistent with these systems having exact isomorphs.

As an example, we perform a direct isomorph check for the asymmetric dumbbell model in Figure 2. A correlation coefficient of  $R = 0.97$  is observed for a 15% density increase. Calculating the temperature of the isomorphic state point from the linear regression slope the result differs only 1% from the prediction by requiring constant excess entropy (see section IV).

In the present paper we show that three model liquids composed of simple rigid molecules have good isomorphs in their phase diagram as defined in eqs 3–5. Section II derives several isomorph invariants in molecular systems composed of rigid molecules. Section III describes the simulation setup and the investigated model systems. Section IV investigates the existence of isomorphs for the asymmetric dumbbell, a symmetric IPL dumbbell, and the Lewis–Wahnström OTP models. Section V investigates the existence of a master isomorph<sup>21</sup> for the asymmetric dumbbell and Lewis–Wahnström OTP models. Section VI summarizes the results and presents an outlook.

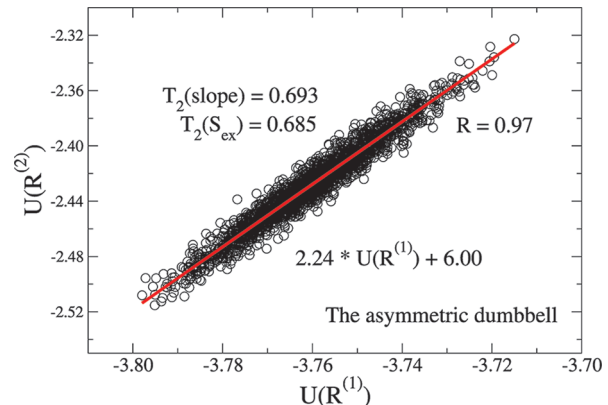


**Figure 2.** “Direct isomorph check”<sup>20</sup> for the asymmetric dumbbell model. During a simulation at state point  $(\rho_1, T_1) = (0.868, 0.309)$  the center-of-mass of each dumbbell is scaled to density  $\rho_2 = 0.999$ , keeping the Eulerian angles fixed. The potential energy is then evaluated from the scaled configurations and plotted against the potential energy of the unscaled configurations. The temperature  $T_2$ (slope) of the isomorphic state point at density  $\rho_2$  is calculated by multiplying the linear regression slope with  $T_1$  (eq 6).  $T_2$ ( $S_{ex}$ ) is the temperature of the isomorphic state point calculated by keeping the excess entropy constant (see section IV). It should be noted that the nonzero constant in the linear regression fit reflects the fact that  $C_{12}$  in general is not unity (eq 6).

## II. ISOMORPH INVARIANTS IN LIQUIDS COMPOSED OF RIGID MOLECULES

From the single assumption of curves of isomorphic state points in an atomic liquid’s phase diagram, ref 20 derived several invariants along an isomorph. Because we have extended this definition in eqs 3–5 to molecular systems composed of rigid molecules, it is natural to wonder which of these invariants can be extended to molecular systems. The molecular isomorph concept is different from the atomic case in that there is no “ideal” reference system (the IPL system). Our simulations, however, show that isomorphs can nevertheless be a useful tool for understanding such liquids.

In the following we derive several invariants from exact isomorphs. We start by noting that the generalization of isomorphs to molecular systems define a bijective map among configurations of state points (1) and (2). The *NVT* configurational probability density for a system of  $N$  rigid molecules is given by<sup>33</sup> (where  $d\mathbf{R} \equiv d\mathbf{r}_{CM,1} d\tau_1 \dots d\mathbf{r}_{CM,N} d\tau_N$  with  $\tau \equiv (\phi, \theta, \chi)$  and  $d\tau = \sin \theta d\theta d\phi d\chi$ <sup>33</sup>)

$$\hat{P}(\mathbf{R}) = \frac{e^{-U(\mathbf{R})/k_B T}}{\int e^{-U(\mathbf{R})/k_B T} d\mathbf{R}} \quad (7)$$

In combination with eq 5 it follows that all mapped configurations of state points (1) and (2) have identical Boltzmann probabilities, i.e.,

$$\hat{P}(\mathbf{R}^{(1)}) d\mathbf{R}^{(1)} = \hat{P}(\mathbf{R}^{(2)}) d\mathbf{R}^{(2)} \quad (8)$$

For convenience we introduce two configurational distribution functions<sup>20,33</sup>

$$P(\mathbf{R}) = (V\Omega)^N \hat{P}(\mathbf{R}) \quad (9)$$

$$\tilde{P}(\tilde{\mathbf{r}}_{CM}^N, \tau^N) = \frac{e^{-U(\rho^{-1/3} \tilde{\mathbf{r}}_{CM}^N, \tau^N)/k_B T}}{\int e^{-U(\rho^{-1/3} \tilde{\mathbf{r}}_{CM}^N, \tau^N)/k_B T} d\tilde{\mathbf{r}}_{CM}^N d\tau^N} \quad (10)$$

where  $\Omega$  is the integral over the Eulerian angles for one molecule ( $\Omega = \int d\tau = 8\pi^2$  for a non-linear molecule).  $P$  has been introduced to make  $\tilde{P}$  dimensionless.  $\tilde{P}(\tilde{\mathbf{r}}_{CM}^N, \tilde{\tau}^N) d\tilde{\mathbf{r}}_{CM}^N d\tilde{\tau}^N$  is the probability to observe the system represented by a point in the volume-element  $d\tilde{\mathbf{r}}_{CM}^N d\tilde{\tau}^N$  located at  $\{\tilde{\mathbf{r}}_{CM}^N, \tilde{\tau}^N\} \equiv \tilde{\mathbf{R}}$ .  $\tilde{P}$  is invariant along an isomorph and is related to  $P$  via  $\tilde{P}(\tilde{\mathbf{r}}_{CM}^N, \tilde{\tau}^N) = (N\Omega)^{-N} P(\mathbf{R}) = \rho^{-N} P(\mathbf{R})$ . We note that the excess entropy  $S_{ex} = -(\partial F_{ex}/\partial T)_{N,V}$ , where  $F_{ex}$  is the excess free energy, can be written as<sup>20</sup>

$$S_{ex} = -k_B \int (V\Omega)^{-N} \ln P(\mathbf{R}) P(\mathbf{R}) d\mathbf{R} \quad (11)$$

$$S_{ex} = -k_B \int \ln \tilde{P} \tilde{P} d\tilde{\mathbf{r}}_{CM}^N d\tilde{\tau}^N - k_B N \ln(N\Omega) \quad (12)$$

From the above observations we now derive a number of isomorph invariants in liquids composed of rigid molecules.

1. *The molecular center-of-mass structure in reduced units.* For a given configuration of the molecular center-of-mass structure in reduced units, all orientations of the molecules of state points (1) and (2) by eq 8 have identical probabilities. The reduced center-of-mass structure is thus invariant along an isomorph.
2. *Any normalized distribution function describing the (relative) orientations of molecules with respect to the reduced center-of-mass structure.* This follows by analogy to statement 1 since all mapped configurations of state points (1) and (2) have identical probabilities.
3. *The isochoric heat capacity  $C_V$ .* The excess heat capacity in the  $NVT$  ensemble is given by  $C_V^{ex} = \langle (\Delta U)^2 \rangle / k_B T^2$ . Defining  $X = U/k_B T$  we may write  $C_V^{ex} = k_B \langle (\Delta X)^2 \rangle$ . By eqs 6 and 8 it follows that  $C_V^{ex}$  is invariant along an isomorph, because the constant  $k_B T_2 \ln C_{12}$  disappears when the mean is subtracted. The ideal gas contribution to  $C_V$  is independent of state point ( $C_V^{id} = 6Nk_B/2$  for non-linear molecule).
4. *The translational two-body entropy*<sup>10,34,35</sup>  $S_t/N = -\rho k_B / 2 \int [g_{CM}(r) \ln g_{CM}(r) - g_{CM}(r) + 1] dr$ , where  $g_{CM}(r)$  is the radial distribution function for the center-of-mass of the molecules. The density dependence disappears when switching to reduced units, and by statement 1 the molecular center-of-mass structure in reduced units is invariant along an isomorph, and thus also the radial distribution function (in reduced units).
5. *The orientational two-body entropy*<sup>10,34,35</sup>  $S_o/N = -\rho k_B / (2\Omega^2) \int g_{CM}(r) g(\omega^2|r) \ln g(\omega^2|r) d\omega^2 dr$ , where  $\omega^2$  denotes a set of angles used to describe the relative orientation of two molecules, and  $g(\omega^2|r)$  is the conditional distribution function for the relative orientation of two molecules separated by a distance  $r$ . Applying reduced units this invariant follows from statements 1 and 2.
6. *All  $N$ -body entropy terms*<sup>34,35</sup> The excess entropy can be expanded as  $S_{ex} = \sum_{i=2}^{\infty} S_i$ . The two-body expression  $S_2 = S_t + S_o$  is given above, whereas the higher-order terms are more involved.
7. *The excess entropy  $S_{ex}$ .* The excess entropy is given by eq 12, and because  $\tilde{P}$  is invariant along the isomorph, so is the excess entropy. The latter also follows from statement 6, because each term is invariant.
8. *The molecular center-of-mass  $NVE$  and Nosé–Hoover  $NVT$  dynamics in reduced units.* The reduced dynamics of the individual atomic positions on account of the constraints is

not invariant along an isomorph. Considering instead the molecular center-of-mass motion the constraint force disappears and these equations of motion are invariant along an isomorph in reduced units. The proof is given in Appendix B (a brief summary of constrained dynamics is given in Appendix A).

9. *Any average molecular center-of-mass dynamic quantity in reduced units.* This follows immediately from statement 8, because the molecular center-of-mass equations of motion in reduced units are invariant along an isomorph. In particular, this would include the reduced relaxation time  $\tilde{\tau}_a$ .

As detailed above, it is necessary to consider the center-of-mass motion and the motion relative to the center-of-mass separately. Nevertheless, during the investigation of isomorphs we will also consider the reduced atomic quantities to examine their “invariance”.

An additional consequence of isomorphs is that, because by eq 8 scaled microconfigurations have identical canonical probabilities, an instantaneous change of temperature and density from an equilibrated state point to an isomorphic state point does not lead to any relaxation. This is called an isomorphic jump.<sup>20</sup>

### III. SIMULATION DETAILS

We studied three model systems of rigid molecules (Figure 3): the asymmetric dumbbell ( $N = 500$ ), a symmetric IPL dumbbell ( $N = 500$ ), and the Lewis–Wahnström OTP models ( $N = 320$ ). The asymmetric dumbbell and Lewis–Wahnström OTP models are composed of LJ atoms, while the symmetric IPL dumbbell model is composed of IPL atoms.

For the LJ models the potential energy  $U$  and the virial  $W$  are given by (equivalent expressions apply for the symmetric dumbbell model)

$$U = U_{LJ} \quad (13)$$

$$W = W_{LJ} + W_{CON} \quad (14)$$

The first term in the virial is the LJ virial  $W_{LJ}$ , the second term is the contribution to the virial due to the constraints (fixed bond lengths),  $W_{CON}$ .  $U_{LJ}$  is a sum over intermolecular pair interactions given by the (12,6)-LJ potential

$$u(r_{ij}) = 4\varepsilon_{\alpha\beta} \left[ \left( \frac{\sigma_{\alpha\beta}}{r_{ij}} \right)^{12} - \left( \frac{\sigma_{\alpha\beta}}{r_{ij}} \right)^6 \right] \quad (15)$$

The potential energy has no contribution from the fixed bonds. A force smoothing procedure<sup>37</sup> was applied from  $r_s = 2.45\sigma_{\alpha\beta}$  to  $r_c = 2.50\sigma_{\alpha\beta}$ , where  $r_c$  is the cut-off distance after which pair interactions are ignored.

The bond lengths were held fixed using the Time Symmetrical Central Difference algorithm,<sup>38,39</sup> which is a central difference time-discretization of the constrained equations of motion preserving time-reversibility. Appendix A gives a brief summary of constrained dynamics and the effect on the virial (see also refs 38, 40, and 41). The simulations were performed in the  $NVT$  ensemble applying the Nosé–Hoover (NH) algorithm<sup>42–44</sup> using RUMD,<sup>45</sup> a molecular dynamics package optimized for state-of-the-art GPU computing.

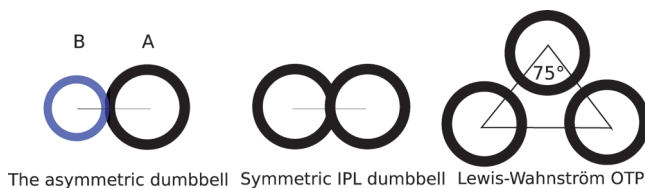


**Figure 3.** Sketch of the three model systems studied: The asymmetric dumbbell, a symmetric IPL dumbbell, and the Lewis–Wahnström OTP models. The asymmetric dumbbell is a simplistic model of toluene with the methyl side group tightly bonded to the benzene molecule. The symmetric IPL dumbbell has the same bond length as the asymmetric dumbbell model. The Lewis–Wahnström OTP model is an isosceles triangle with an angle of 75°, different from the 60° of the real 1,2-diphenylbenzene molecule.<sup>36</sup>

The *NVT* simulations were performed without adjusting the time constant of the NH algorithm (see Appendix B). This choice is not expected to influence the results over the observed density and temperature range, because the dynamics is not particularly sensitive to the absolute value of the NH time constant.<sup>46</sup> The specific details of the investigated models follow below.

**A. The Asymmetric Dumbbell.** The asymmetric dumbbell model consists of a large (A) and small (B) LJ particle, rigidly bonded with a bond distance of  $r_{ij} = 0.584$  (here and henceforth units are given in LJ units referring to the A particle,  $\sigma_{AA} = 1$ ,  $\epsilon_{AA} = 1$ , and  $m_A = 1$ ). The parameters were chosen to roughly mimic toluene.<sup>22</sup> The asymmetric dumbbell model can be cooled to a highly viscous state without crystallizing, making it feasible to study slow dynamics. The asymmetric dumbbell model has  $\sigma_{AB} = 0.894$ ,  $\sigma_{BB} = 0.788$ ,  $\epsilon_{AB} = 0.342$ , and  $\epsilon_{BB} = 0.117$  with  $m_B = 0.195$ .

**B. Symmetric IPL Dumbbell.** The symmetric IPL dumbbell model consists of two identical particles, rigidly bonded with bond distance of  $r_{ij} = 0.584$ . The atoms in different molecules interact via an IPL potential with exponent  $n = 18$ . The masses and IPL parameters are set to unity and a cut-and-shifted potential at  $r_c = 2.50$  is applied.

**C. Lewis–Wahnström OTP.** The Lewis–Wahnström OTP model<sup>29,30</sup> consists of three identical LJ particles rigidly bonded together in an isosceles triangle with sides of  $r_{ij} = 1.000$  and top-angle of 75°, i.e., different from the 60° of the real 1,2-diphenylbenzene molecule.<sup>36</sup> All LJ parameters (including the masses) are unity for the OTP model.

#### IV. NUMERICAL STUDY OF ISOMORPHS FOR THE THREE MODEL SYSTEMS

To investigate whether the three model systems have good isomorphs, we first describe how to generate an isomorph in a simulation. The excess entropy  $S_{\text{ex}}$  is invariant along an isomorph, and the method for generating an isomorph is to generate a curve of constant  $S_{\text{ex}}$  (see section II and also refs 20 and 21). A curve of constant excess entropy can be found by using the exact *NVT* ensemble relation<sup>20</sup>

$$\frac{\langle \Delta U \Delta W \rangle}{\langle (\Delta U)^2 \rangle} = \left( \frac{\partial \ln T}{\partial \ln \rho} \right)_{S_{\text{ex}}} \equiv \gamma \quad (16)$$

In simulations an isomorph is generated as follows: (1) The left-hand side is calculated from the fluctuations at a given state point. (2) A new state point is identified by a discretization of eq 16 changing the density by 1%, and the new

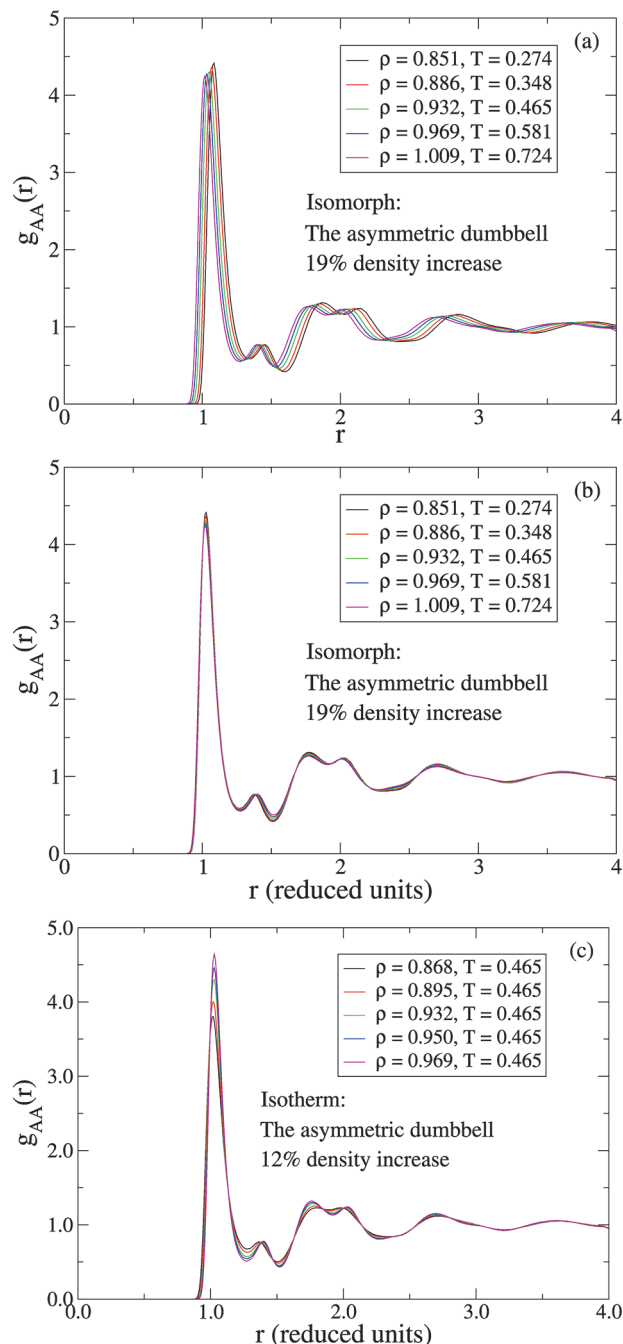


**Figure 4.** Radial distribution functions for the asymmetric dumbbell model. (a) AA pair-correlation function along an isomorph with 19% density increase before scaling the distance  $r$  into reduced units. (b) AA pair-correlation function along the same isomorph after scaling the distance  $r$  into reduced units. (c) AA pair-correlation function along an isotherm with 12% density increase after scaling of the distance into reduced units.

temperature is calculated from  $\Delta \ln T = \gamma \Delta \ln \rho$ . (3) The procedure is repeated and in this way an isomorph is generated in the phase diagram.

**A. Isomorphs of the Asymmetric Dumbbell Model.** This section investigates the asymmetric dumbbell model. Isomorphs were mapped out following the procedure described above. Figure 4 shows the AA radial distribution functions along an isomorph with 19% density increase before (a) and after (b) scaling the distance  $r$  into

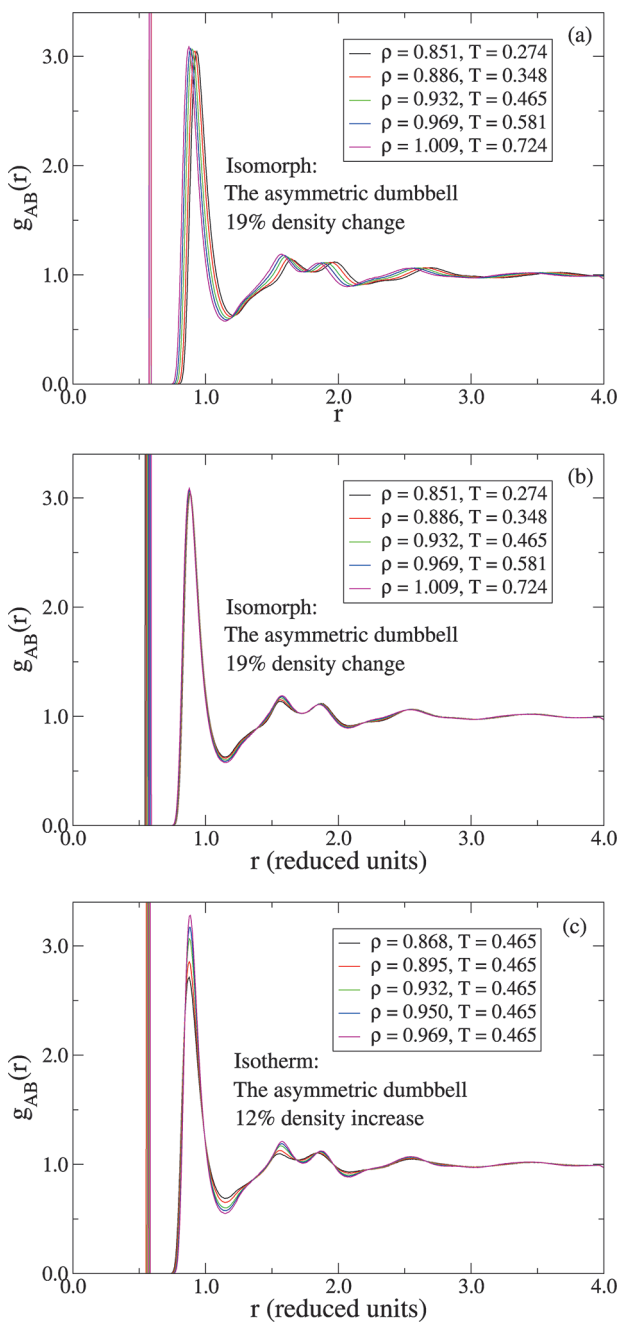


**Figure 5.** Radial distribution functions for the asymmetric dumbbell model. (a) AB pair-correlation function along the isomorph of Figure 4 before scaling the distance  $r$  into reduced units. (b) AB pair-correlation function along the same isomorph after scaling the distance  $r$  into reduced units. (c) AB pair-correlation function along the isotherm of Figure 4 after scaling of the distance into reduced units.

reduced units via

$$\tilde{r} = \rho^{1/3} r \quad (17)$$

Also shown for reference in Figure 4c is the AA radial distribution functions along an isotherm with 12% density increase. Although the reduced structure of the atomic positions, due to the fixed bonds, is predicted not to be invariant along an isomorph, Figure 4 shows that it nevertheless is so to a reasonable approximation. The

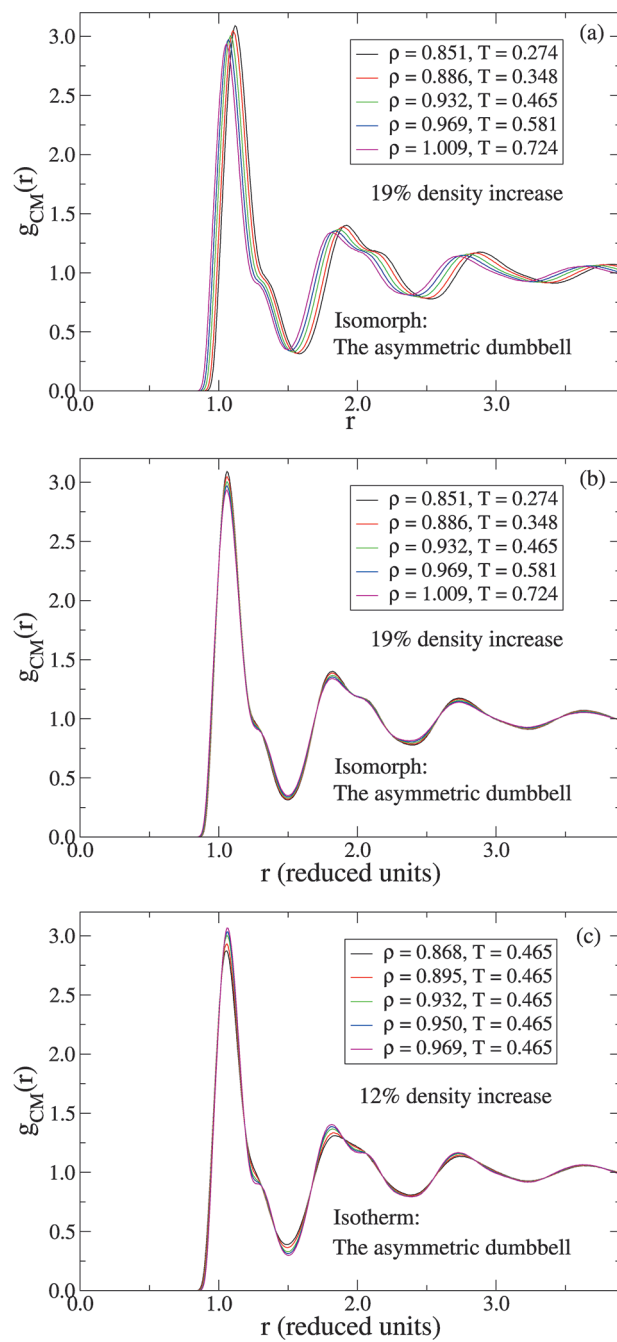


**Figure 6.** Molecular center-of-mass radial distribution functions for the asymmetric dumbbell model. (a) Pair-correlation function along the isomorph of Figures 4 and 5 before scaling the distance  $r$  into reduced units  $\tilde{r} = \rho^{1/3} r$ . (b) Pair-correlation function along the same isomorph after scaling the distance  $r$  into reduced units. (c) Pair-correlation function along the isotherm of Figures 4 and 5 after scaling of the distance into reduced units.

reduced structure of the atomic positions is less invariant along the isotherm. Figure 5 considers the AB radial distribution functions, where the constrained bond distance shows up as a sharp peak. The analogous conclusion as with the AA distribution functions is reached, and likewise for the BB distribution functions (not shown).

Next, we consider in Figure 6 the molecular center-of-mass radial distribution functions along the isomorph and isotherm of Figures 4 and 5. This quantity is predicted to be invariant along

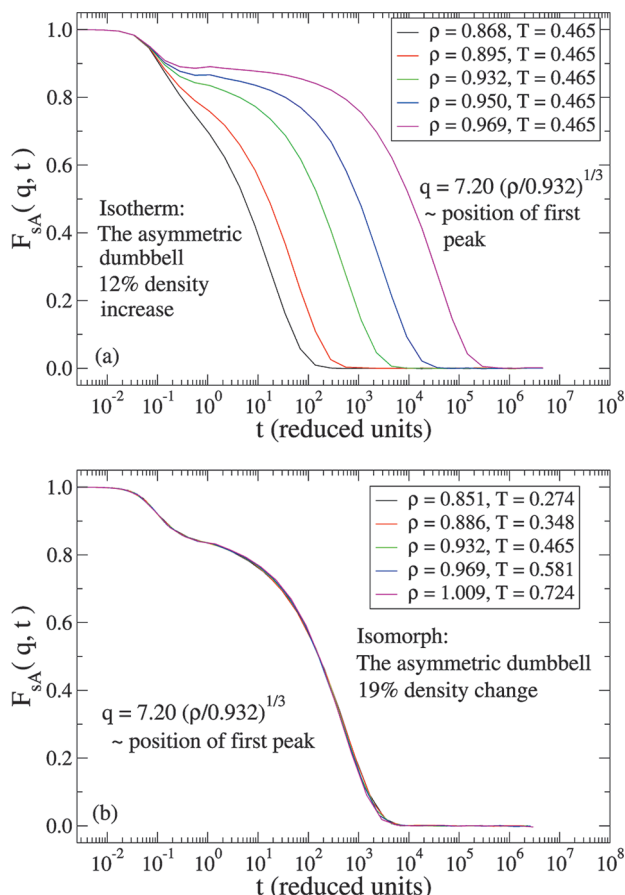


**Figure 7.** Reduced A-particle incoherent intermediate scattering functions for the asymmetric dumbbell model keeping the reduced wavevector  $q$  constant. (a) Along the isotherm of Figures 4–6 with 12% density increase. (b) Along the isomorph of Figures 4–6 with 19% density increase.

an isomorph (see section II). The molecular center-of-mass structure is to a good approximation invariant in reduced units along the isomorph, but this is less so along the isotherm, as can be seen from the first and second peaks. It should, however, be noted that beyond  $r \approx 2.3$  the isotherm appears more invariant than the isomorph.

We consider in Figure 7 the dynamics in terms of the reduced A-particle incoherent intermediate scattering function. The reduced dynamics of the atoms is not predicted to be invariant along an isomorph (see Appendix B); however, the figure shows that it is a good approximation. The same conclusion is reached for the B-particle (not shown). In Figure 8 we consider the reduced molecular center-of-mass self-part of the intermediate scattering function. This quantity is predicted to be invariant along an isomorph (see Appendix B), and Figure 8 clearly shows this. The dynamics is not invariant along the isotherm.

We show the variation of  $\gamma$ , calculated from the NVT fluctuations via eq 16, in Figure 9 along an isochoore and along the isomorph of Figures 4–8 in two different versions. The crosses show  $\gamma$  calculated from the total virial  $W$ , and the asterisks show  $\gamma$  calculated after subtracting the constraint contribution to virial, i.e., replacing  $W$  with  $W_{\text{LJ}} = W - W_{\text{CON}}$ . Reference 20 predicts that  $\gamma$  should be a function of density only  $\gamma = \gamma(\rho)$ . This is seen

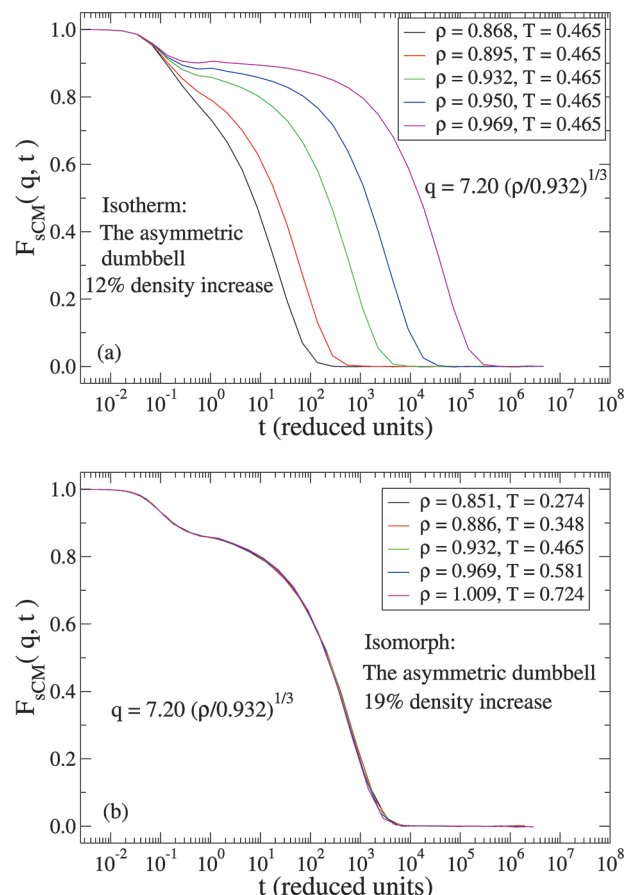


**Figure 8.** Reduced molecular center-of-mass incoherent intermediate scattering functions for the asymmetric dumbbell model keeping the reduced wavevector  $q$  constant. (a) Along the isotherm of Figures 4–7 with 12% density increase. (b) Along the isomorph of Figures 4–7 with 19% density increase.

in Figure 9 to be a good approximation for both versions of  $\gamma$ , where the crosses are the  $\gamma$  used to keep the excess entropy constant. The  $\gamma$  calculated from the LJ virial is seen to be lower than the  $\gamma$  calculated from the total virial. The  $\gamma$  derived from the LJ virial is related to an effective IPL exponent that reproduces the structure and the dynamics of the molecular liquid (see ref 47 for more details).

As mentioned in the Introduction, density scaling<sup>1–3</sup> is the empirical observation that the reduced relaxation time  $\tilde{\tau}_\alpha$  for many viscous liquids can be written as some function  $\tilde{\tau}_\alpha = f(\rho^{\gamma_{\text{scale}}}/T)$  where  $\gamma_{\text{scale}}$  in experiments is a fitting exponent. If we assume that  $\gamma$  is constant along an isomorph, eq 16 implies that  $\rho^\gamma/T = \text{const}$  describes the isomorph. In this case density scaling will hold to a good approximation because the reduced relaxation time is an isomorph invariant; for the dumbbell system  $\gamma$  changes only moderately along an isomorph and thus density scaling is a fair approximation for this system.<sup>22</sup> That  $\gamma$  for systems with isomorphs can be identified with the density scaling exponent  $\gamma_{\text{scale}}$  has very recently been verified experimentally for a silicone oil.<sup>31</sup>

Starting from an equilibrated sample at some state point, changing either temperature or density alters the equilibrium Boltzmann distribution of states. Two isomorphic state points have identical canonical probabilities of scaled microconfigurations

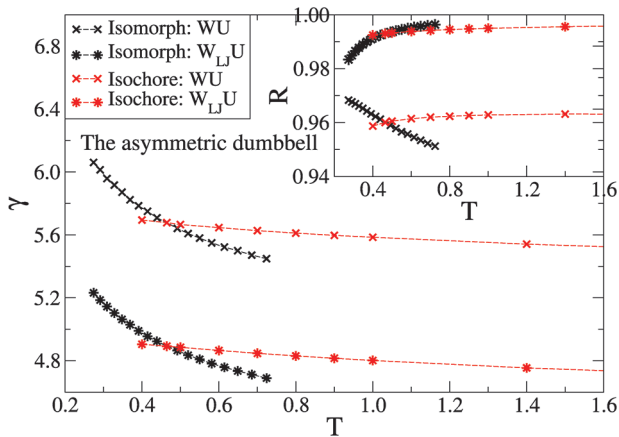


**Figure 9.** Variation of  $\gamma$  (eq 16) and the correlation coefficient  $R$  (eq 1) for the asymmetric dumbbell model in two different versions along an isochore (red,  $\rho = 0.932$ ) and along the isomorph (black) of Figures 4–8. The crosses show  $\gamma$  calculated from the total virial  $W$ , and the asterisks show  $\gamma$  calculated after subtracting the constraint contribution to virial, i.e.,  $W_{\text{LJ}} = W - W_{\text{CON}}$ . The corresponding  $R$ 's are shown in the inset.  $\gamma$  is predicted in ref 20 to be a function only of density, which is seen to apply to a good approximation for both versions.

(eq 8). A sudden change of state from an equilibrated state point to an isomorphic state point should thus not lead to any relaxation. This is called an isomorphic jump, and the prediction of no relaxation was shown in ref 20 to work well for the KABLJ liquid.

A similar numerical experiment is carried out for the asymmetric dumbbell model in Figure 10. Considering three equilibrated, isochoric state points (1), (2), and (3), density and temperature are instantaneously changed to a state point (4). State point (4) is isomorphic to state point (2). The isomorph prediction is that jumps from state points (1) and (3) show relaxation, whereas jumps from state point (2) do not. This is indeed the case (Figure 10a). State point (1) ages from below because the aging scheme (1)  $\rightarrow$  (4) can be described as first an instantaneous isomorphic jump to the correct density, but a lower temperature, and subsequently relaxation from this state point along the isochore of state point (4).

We finally consider the excess isochoric heat capacity per particle  $C_V^{\text{ex}}/N$  in Figure 11 along the isomorph and isotherm of Figures 4–8. The excess heat capacity increases less than 2% along the isomorph, whereas the 12% density increase on the isotherm results in a 25% increase in the excess heat capacity. This is consistent with the prediction in section II that  $C_V^{\text{ex}}/N$  is an isomorph invariant.

The previous figures show that isomorphs exists to a good approximation for the asymmetric dumbbell model. An important question is whether the specific molecular geometry determines whether or not a particular LJ model has good isomorphs. In Figure 12 the correlation coefficient  $R$  is given as a function of the bond length. The correlation coefficient decreases to  $R \approx 0.65$  at unity bond length, and one might be tempted to conclude that LJ models with large bonds lengths in general do not have good isomorphs. In section IV C we investigate the Lewis–Wahnström OTP model that have unity bond lengths and show that this model actually has good isomorphs. A theory relating the variation of  $R$  to the molecular geometry and/or bond lengths remains to be developed.

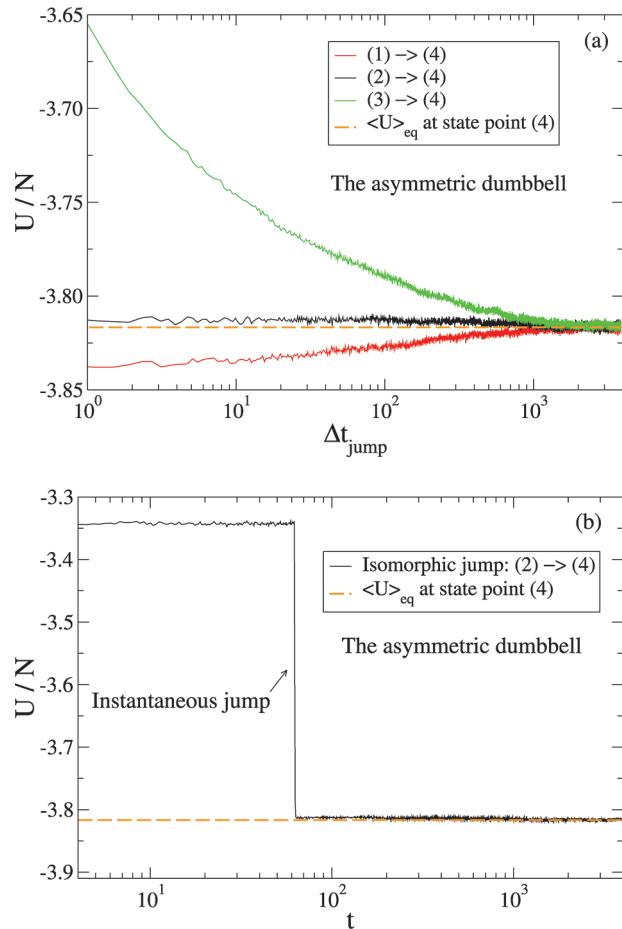


**Figure 10.** Four state points (1), (2), (3), and (4) corresponding to, respectively,  $(\rho, T) = (0.932, 0.400)$ ,  $(0.932, 0.465)$ ,  $(0.932, 2.000)$ , and  $(0.851, 0.274)$  are given where the first three state points are on the same isochore. State points (2) and (4) are isomorphic, whereas (1) and (3) are not isomorphic to (4). After equilibrating at state points (1), (2), and (3), respectively, temperature and density are instantaneously changed to that of state point (4) via a scaling of the center-of-mass coordinates keeping the Eulerian angles of the molecules fixed. An average has been performed over 100 samples. (a) Relaxational behavior of all state points quantified by the potential energy  $U$ . The isomorph jump (2)  $\rightarrow$  (4) shows no relaxation whereas the other state points do. (b) Close up of the potential energy of state point (2) before and after the jump, where the jump takes place at  $t \approx 60$ .

**B. Isomorphs of a Symmetric IPL Dumbbell Model.** In this section we briefly consider a symmetric IPL dumbbell model (see section III B). In Figures 13a,b we show the particle radial distribution functions along an isomorph before and after scaling the distance  $r$  into reduced units. Also shown is the reduced particle incoherent intermediate scattering function in Figure 13c. The corresponding molecular center-of-mass quantities are shown in Figure 14. The atomic dynamics of Figure 13c appear slightly more invariant than the reduced molecular center-of-mass dynamics of Figure 14c, and the difference seems to be larger than what can be contributed to statistics. The latter is predicted to be invariant along an isomorph whereas the former is not. However, we have not tried to quantify this observation any further.

Atomic systems with IPL interactions have exact isomorphs. This reflects the scale invariance of the IPL potential, i.e., that it

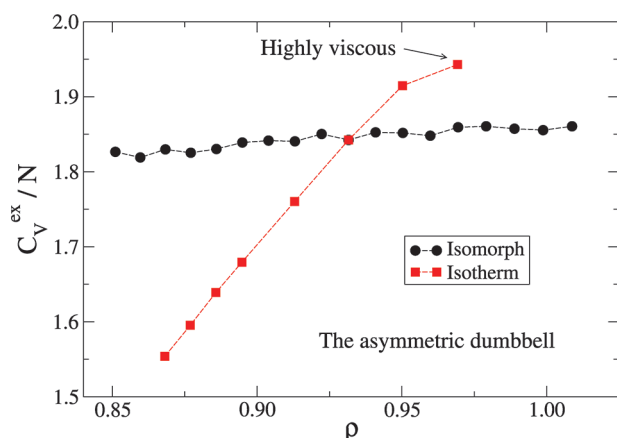


**Figure 11.** Excess isochoric heat capacity per particle  $C_V^{\text{ex}}/N$  for the asymmetric dumbbell model as a function of density along the isomorph (black) and isotherm (red,  $T = 0.465$ ) of Figures 4–8. The density increase is 19% and 12%, respectively. Consistent with the predicted isomorph invariance, the excess isochoric heat capacity increases less than 2% along the isomorph, whereas the isotherm shows a 25% increase. For the isotherm the dynamics becomes very slow for densities higher than  $\rho = 0.950$  and the system becomes difficult to equilibrate properly.

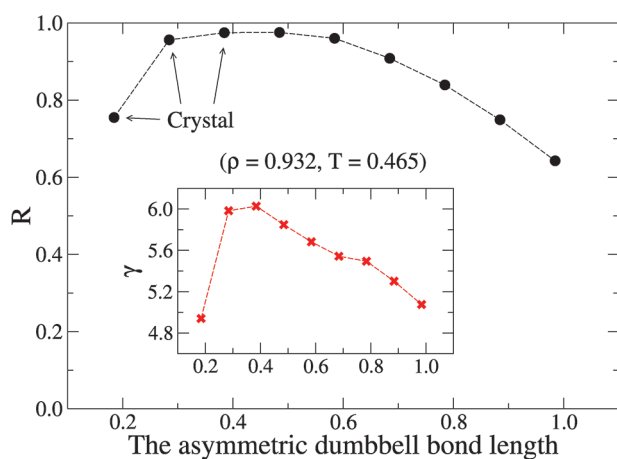


**Figure 12.** Correlation coefficient  $R$  as a function of the bond length in the asymmetric dumbbell model at  $(\rho, T) = (0.932, 0.465)$ . The investigated model has bond length 0.584 with a correlation coefficient  $R \approx 0.97$ ; however, as the bond length increases, the correlation coefficient decreases to  $R \approx 0.65$  at unity bond length. The inset shows the corresponding values of  $\gamma$  as defined in eq 16. As the bond length increases, the system becomes very viscous and the statistics is poor at high bond lengths.

preserves its shape under a scaling of the argument. Because molecules by their fixed geometry define a length scale in the system, isomorphs will always be approximate. However, the previous figures show that rigid molecules with IPL intermolecular interactions can also have good isomorphs.

In Figure 15 we consider the variation of  $\gamma$  and  $R$  along the investigated isomorph, which shows that  $R$  decreases slightly with increasing temperature (and density). The variation of  $\gamma$  along the isomorph is less than for the asymmetric dumbbell, and  $\gamma$  is to a good approximation constant. As for the asymmetric dumbbell model (Figure 9), the effect of the constraints is to increase  $\gamma$  and decrease  $R$  (these are, respectively, 6 and 1 for the atomic IPL potential used).

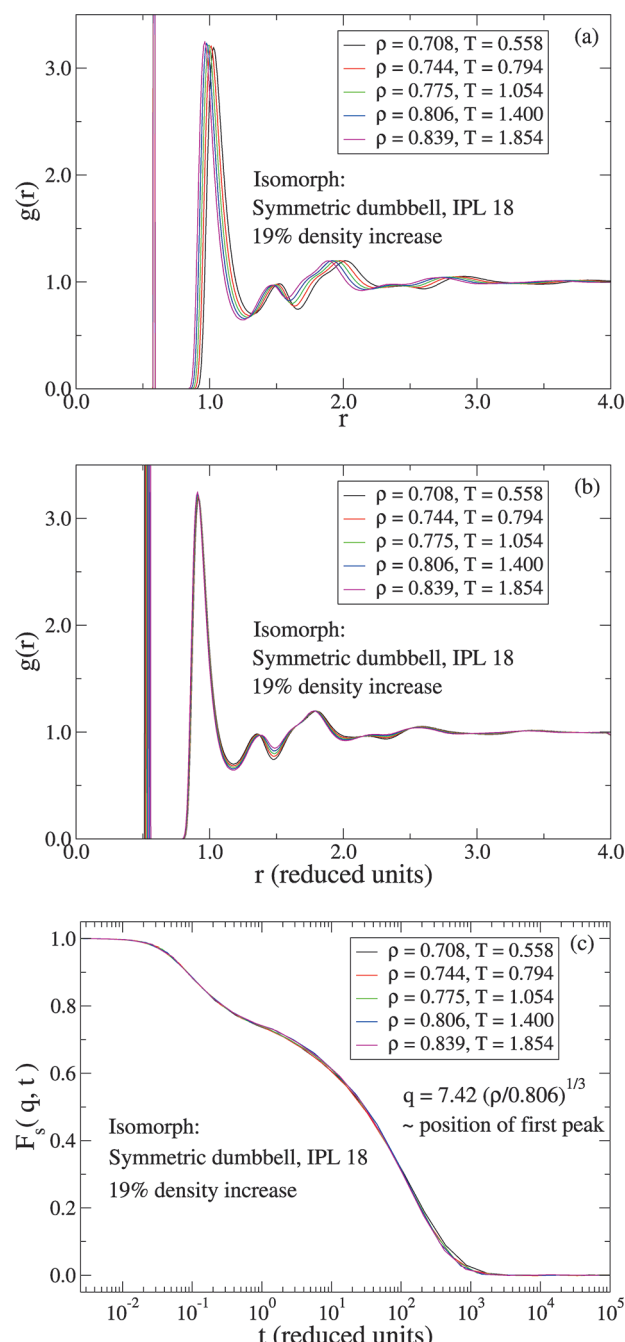


**Figure 13.** Structure and dynamics along an isomorph with 19% density increase for the symmetric IPL dumbbell model ( $n = 18$ ). (a) Particle pair-correlation functions before scaling the distance  $r$  into reduced units. (b) Particle pair-correlation functions after scaling the distance  $r$  into reduced units. (c) The reduced particle incoherent intermediate scattering functions at constant reduced wavevector  $q$ .

**C. Isomorphs of the Lewis–Wahnström OTP Model.** We proceed to investigate the Lewis–Wahnström OTP model.<sup>29,30</sup> Figure 16 shows the particle radial distribution functions along an isomorph with 21% density increase before and after scaling the distance  $r$  into reduced units. We treat the particles as identical in the quantities probed in simulations (i.e., the radial distribution function, etc.) even though the OTP model is an isosceles triangle. Also shown for reference is an isotherm with 11%

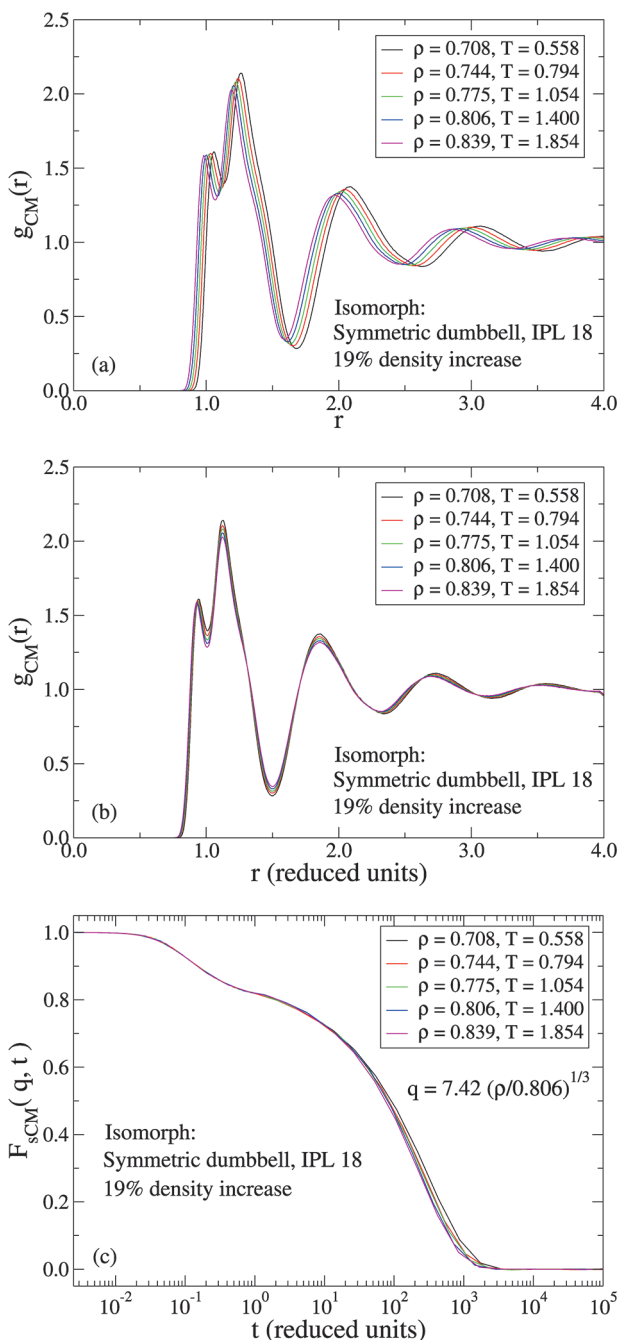


**Figure 14.** Structure and dynamics along the isomorph of Figure 13 for the symmetric IPL dumbbell model ( $n = 18$ ). (a) Molecular center-of-mass pair-correlation functions before scaling the distance  $r$  into reduced units  $\tilde{r} = \rho^{1/3} r$ . (b) Molecular center-of-mass pair-correlation functions after scaling the distance  $r$  into reduced units. (c) Reduced molecular center-of-mass incoherent intermediate scattering functions at constant reduced wavevector  $q$ .

density increase in Figure 16c. Figure 17 shows the corresponding reduced molecular center-of-mass radial distribution functions. The reduced molecular center-of-mass structure is less invariant along the isomorph than for the asymmetric dumbbell (Figure 6), consistent with the OTP model being less strongly correlating ( $R \approx 0.90$ ). However, comparing with the isotherm in Figure 17c, the OTP model, here, crystallizes at the highest density probed,<sup>36</sup> even though the density increase is just 11% compared with the 21% density increase along the isomorph.

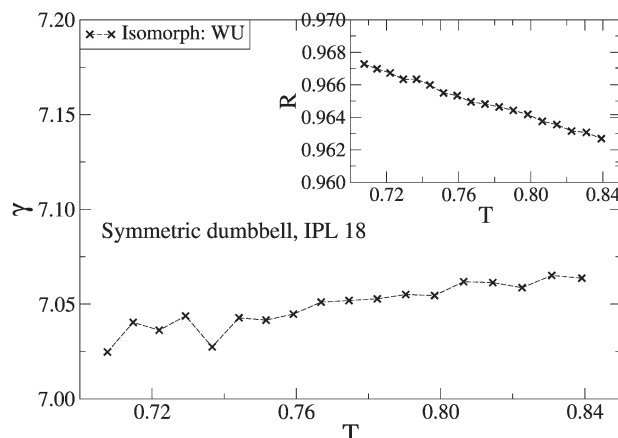


**Figure 15.** Variation of  $\gamma$  and  $R$  (inset) along the isomorph of Figures 13 and 14 with a 19% density increase for the symmetric IPL dumbbell model ( $n = 18$ ).  $\gamma$  increases slightly along the isomorph. Excluding the constraints in the virial correlation coefficient and  $\gamma$  are respectively  $R = 1$  and  $\gamma = 6$ .

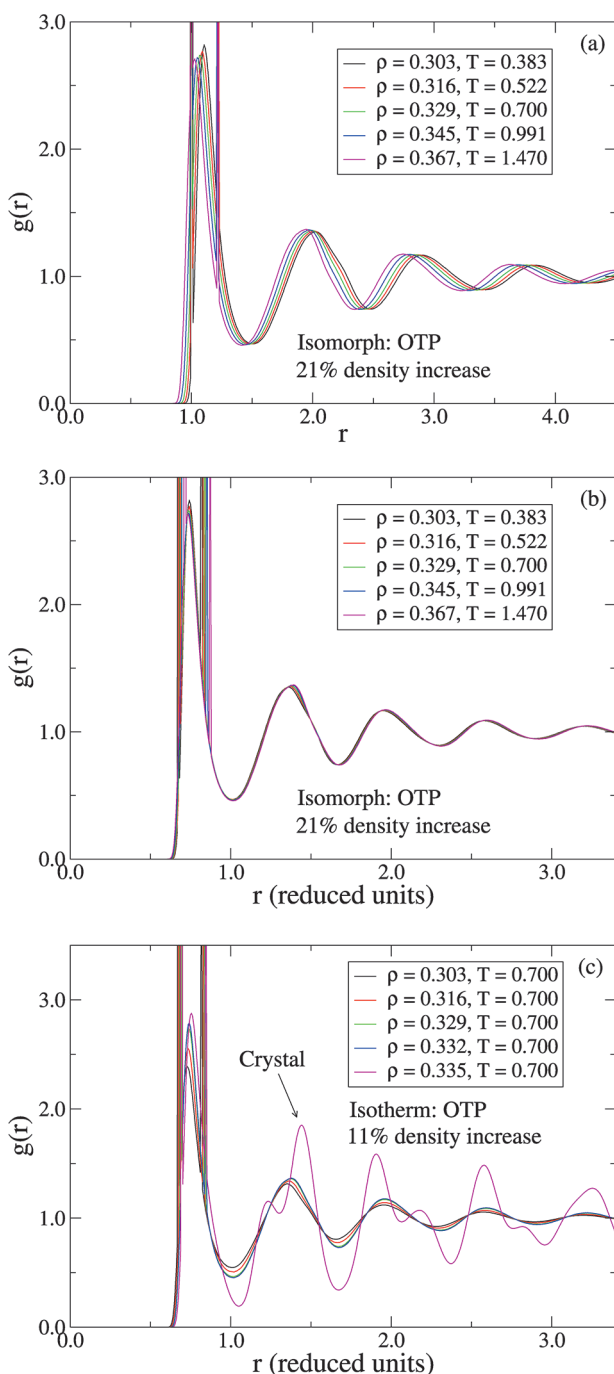
Comparing now with the particle quantities of Figure 16, the latter seems to be more invariant along the isomorph, even though the reduced molecular center-of-mass structure is predicted in section II to be invariant. The isomorph invariants presented in section II are exact in the case of exact isomorphs; however, the OTP model has a correlation coefficient of 0.90, and we expect this to be the cause of disagreement. This, however, does not explain why the reduced structure should be more invariant, and we currently have no explanation for this.

Figure 18 shows the reduced particle incoherent intermediate scattering functions along the isotherm and isomorph of Figures 16 and 17, while Figure 19 shows the reduced molecular center-of-mass incoherent intermediate scattering functions. For the molecular quantities, the dynamics is roughly invariant along the isomorph but not on the isotherm, even though the density increase is 21% for the isomorph and only 11% for the isotherm. In contrast to the reduced molecular center-of-mass structure; the molecular dynamics (Figure 19b) is just as invariant as the particle dynamics (Figure 18b), consistent with the prediction of section II.

We consider in Figure 20 the variation of  $\gamma$  as defined by eq 16. The large variation in  $\gamma$  indicates that density scaling may show a breakdown sooner (for a given change in density) for the Lewis–Wahnström OTP model than for the asymmetric dumbbell where  $\gamma$  changes less along an isomorph. The isomorphs of the OTP model are, however, more approximative than for the asymmetric dumbbell, which is consistent with OTP model being less strongly correlating.

Next, we consider isomorph jumps for the OTP model. The setup is analogous to that of the asymmetric dumbbell model described in section IV A. It is seen from Figure 21 that an isomorph jump shows no relaxation. The apparent larger fluctuations in the potential energy (Figure 21b) than for the asymmetric dumbbell (Figure 10b) are due to a change of scale in the figure.

We close the investigation of the OTP model by considering in Figure 22 the isochoric excess heat capacity per particle  $C_V^{\text{ex}}/N$ . This quantity increases 7% over the 21% density increase along the isomorph, whereas the 11% density increase on the isotherm results in a 34% increase in the isochoric excess heat capacity before crystallizing. These results are consistent with the prediction that  $C_V^{\text{ex}}$  is an isomorph invariant (see section II), although less so than for the asymmetric dumbbell model.



**Figure 16.** Particle radial distribution functions for the OTP model. (a) Along an isomorph with 21% density increase, shown prior to scaling the distance  $r$  into reduced units. (b) Along the same isomorph after scaling the distance  $r$  into reduced units. (c) Along an isotherm with 11% density increase. At the highest density probed the OTP model crystallizes<sup>36</sup> (magenta).

## V. MASTER ISOMORPHS

The previous section detailed the existence of isomorphs in the phase diagram of liquids of small rigid molecules. We now investigate whether the generated isomorphs for the LJ systems have the same shape in the *WU* phase diagram, i.e., whether a so-called master isomorph exists, as has been shown for generalized LJ atomic systems.<sup>21</sup> It is also interesting to compare the isomorphs of the asymmetric dumbbell and OTP models, because

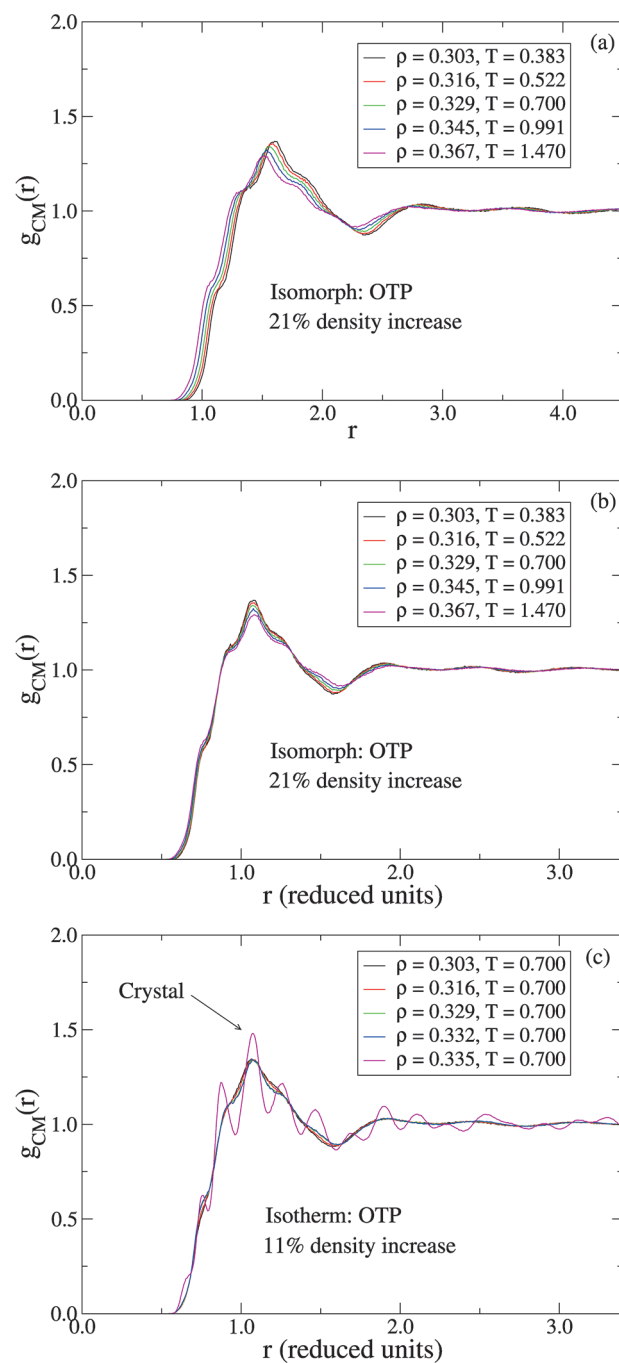


**Figure 17.** Molecular center-of-mass radial distribution functions for the OTP model. (a) Along the isomorph of Figure 16 with 21% density increase, shown prior to scaling the distance  $r$  into reduced units. (b) Along the same isomorph after scaling the distance  $r$  into reduced units. (c) Along the isotherm of Figure 16 with 11% density increase. At the highest density probed the OTP model crystallizes (magenta).

both systems have intermolecular (12,6)-LJ interactions, but different constraint contributions to the virial (one versus three constrained distances per molecule).

Figure 23a shows three different isomorphs in the *WU* phase diagram for the asymmetric dumbbell model, in two different versions: one for the total virial  $W$  and one for the "LJ" virial, i.e., replacing  $W$  by  $W_{LJ} = W - W_{CON}$ . To investigate whether a master isomorph exists, Figure 23b shows the same isomorphs

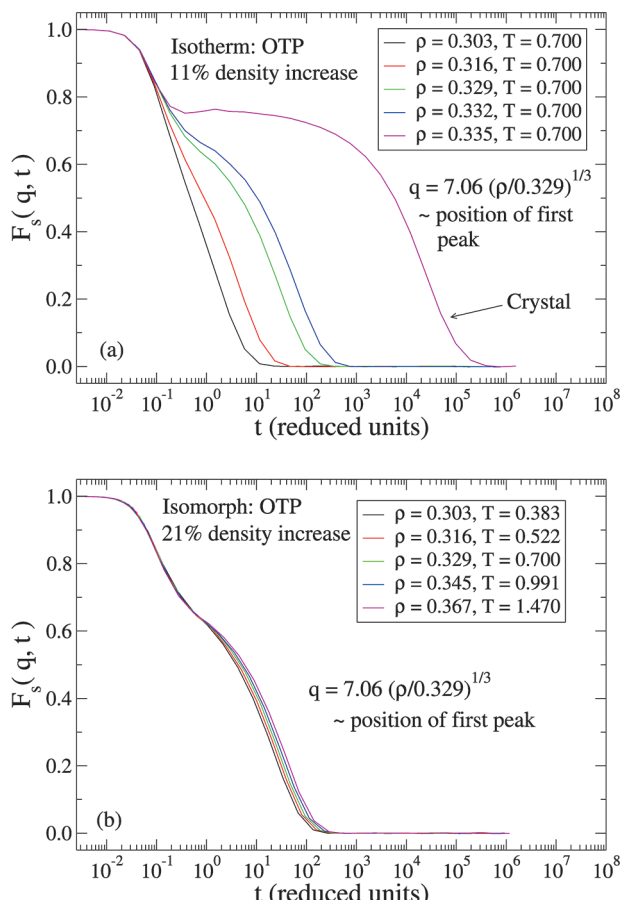


**Figure 18.** The reduced particle incoherent intermediate scattering functions for the OTP model keeping the reduced wavevector  $q$  constant. (a) Along the isotherm of Figures 16 and 17 with 11% density increase. (b) Along the isomorph of Figures 16 and 17 with 21% density increase and almost a factor of 4 increase in temperature. The dynamics is roughly invariant along the isomorph, but not along the isotherm.

after scaling of the potential energy and the virial with the *same* factor (depending on the isomorph). The best scaling factor was identified by trial and error. Corresponding figures for the OTP model are given in Figure 24. The figures show that for both models a master isomorph exists to a good approximation both with and without the constraint contribution to the virial.

Reference 21 derived predictions concerning the shape of isomorphs for *atomic* systems with pair potential given by a sum of two IPLs (the generalized LJ potential). The question arises whether  $W_{\text{LJ}}U$  follows that shape? This is studied in Figure 25a where the  $W_{\text{LJ}}U$  isomorphs for the asymmetric dumbbell and OTP models are scaled using the previously mentioned procedure. The two dashed curves are the isomorph prediction for an *atomic* (12,6)-LJ system<sup>21</sup> (where  $\tilde{\rho} = \rho/\rho^*$  and  $\rho^*$  is the density of a chosen reference state point)

$$U = U_m^* \tilde{\rho}^4 + U_n^* \tilde{\rho}^2 \quad (18)$$

$$W_{\text{LJ}} = 4U_m^* \tilde{\rho}^4 + 2U_n^* \tilde{\rho}^2 \quad (19)$$

where the reference coefficients ( $U_m^*$ ,  $U_n^*$ ) have been calculated from two different state points along “Isomorph 1” of the asymmetric dumbbell.<sup>21</sup> The only assumption used in ref 21 to

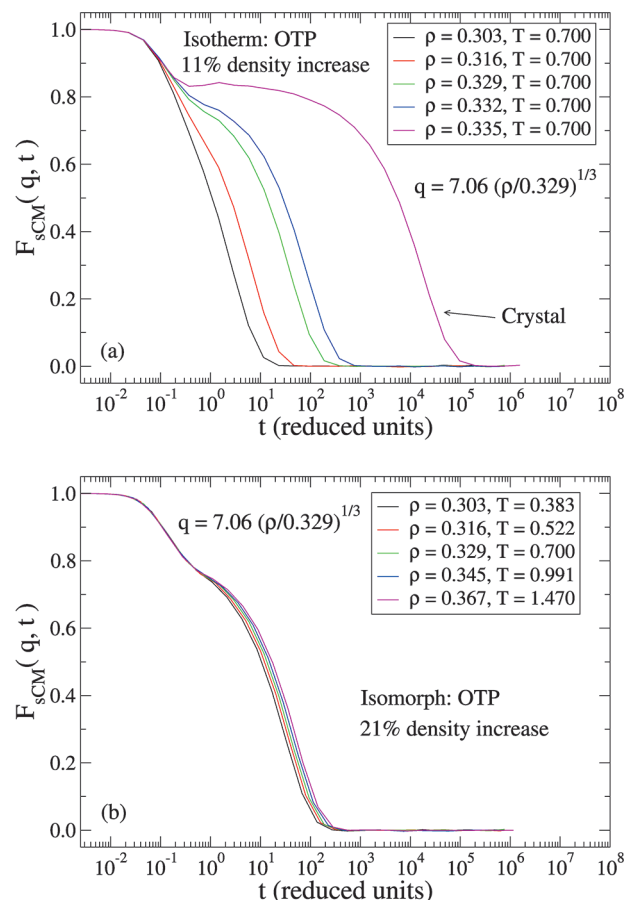


**Figure 19.** Reduced molecular center-of-mass incoherent intermediate scattering functions for the OTP model keeping the reduced wavevector  $q$  constant. (a) Along the isotherm of Figures 16–18 with 11% density increase. (b) Along the isomorph of Figures 16–18 with 21% density increase and almost a factor of 4 increase in temperature. The dynamics is roughly invariant along the isomorph, but not along the isotherm.

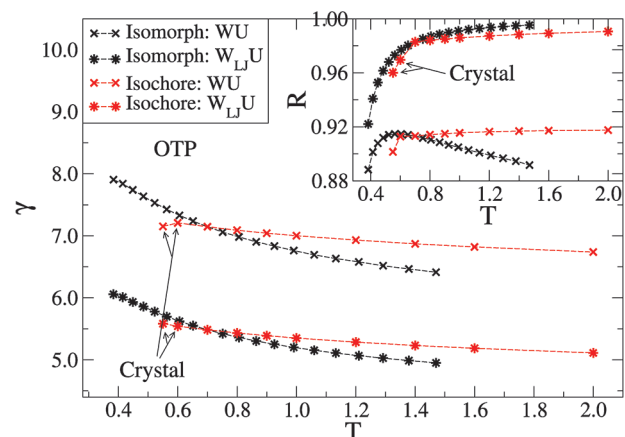


**Figure 20.** Variation of  $\gamma$  (eq 16) and the correlation coefficient  $R$  (inset, eq 1) for the OTP model in two different versions along an isochore (red,  $\rho = 0.329$ ) and the isomorph (black) of Figures 16–19. The crosses show  $\gamma$  calculated from the total virial  $W$ , the asterisks show  $\gamma$  calculated after subtracting the constraint contribution to virial, i.e., replacing  $W$  by  $W_{\text{LJ}} = W - W_{\text{CON}}$ .  $\gamma$  is predicted in ref 20 to be a function only of density as is seen to be the case for both versions, although the variation is larger than for the asymmetric dumbbell.

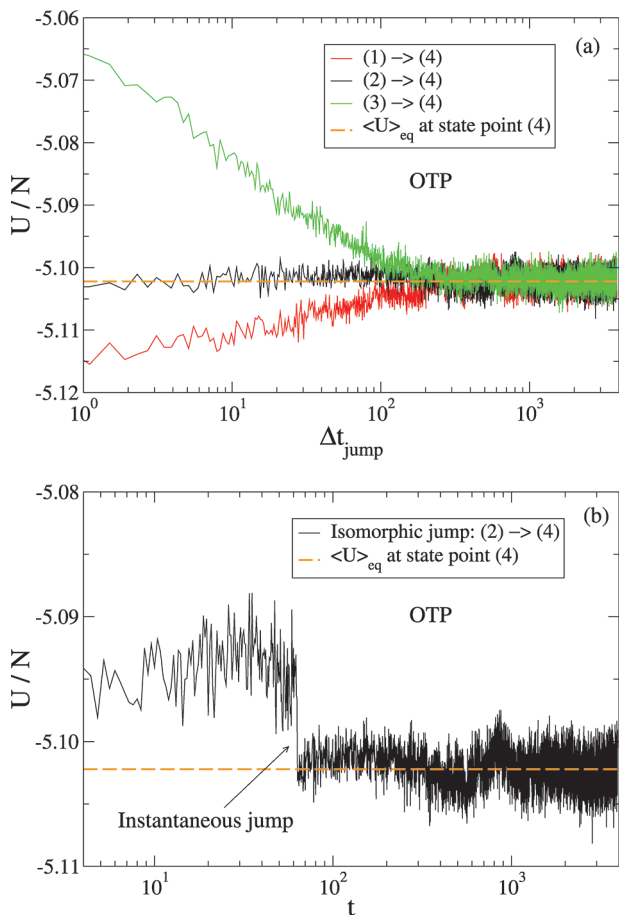


**Figure 21.** Four state points (1), (2), (3), and (4) corresponding to, respectively,  $(\rho, T) = (0.329, 0.650)$ ,  $(0.329, 0.700)$ ,  $(0.329, 1.000)$ , and  $(0.303, 0.383)$  are given where the first three state points are on the same isochore. State points (2) and (4) are isomorphic whereas (1) and (3) are not isomorphic to (4). After equilibrating at state points (1), (2), and (3), respectively, the temperature and density are instantaneously changed to that of state point (4) via a scaling of the center-of-mass coordinates keeping the Eulerian angles of the molecules fixed. An average has been performed over 100 samples. (a) Relaxational behavior of all state points quantified by the potential energy  $U$ . The isomorph jump  $(2) \rightarrow (4)$  shows no relaxation whereas the other jumps do. (b) Close up of the potential energy of state point (2) before and after the jump, where the jump takes place at  $t \approx 60$ .

derive these formulas is the invariance of the reduced atomic structure along an isomorph; however, this is not predicted to be the case for molecular systems with isomorphs (see section II).

It is clear that the atomic isomorph shape is not followed exactly. Nevertheless, there seems to exist not only a master isomorph in the LJ and total virial for the individual systems, but also for the LJ virial between these two different model systems. The same does not hold for the total virial, as can be seen in Figure 25b, because the constraint contributions are different.

To examine the extent of “deviation” from eqs 18 and 19, we show in Figure 26 for the asymmetric dumbbell  $U/\tilde{\rho}^2$  and  $W_{\text{LJ}}/\tilde{\rho}^2$  as functions of the reduced density  $\tilde{\rho}^2$  ( $\rho^* = 1$ ). The reference coefficients can be calculated from a linear regression fit of the potential energy and the estimated coefficients can be used to plot a straight line in the LJ virial plot. This is performed in Figure 26 where it is clear that even though both plots follow a

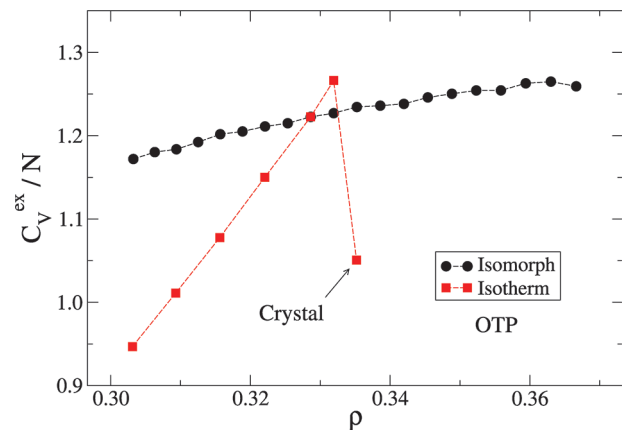


**Figure 22.** Isochoric excess heat capacity per particle  $C_V^{\text{ex}}/N$  for the OTP model as a function of density along the isomorph (black) and isotherm (red) of Figures 16–19. The density increase is 21% and 11%, respectively. At high densities for the isotherm the OTP model crystallizes. The isochoric excess heat capacity is to a good approximation invariant along the isomorph, whereas this is not the case for the isotherm.

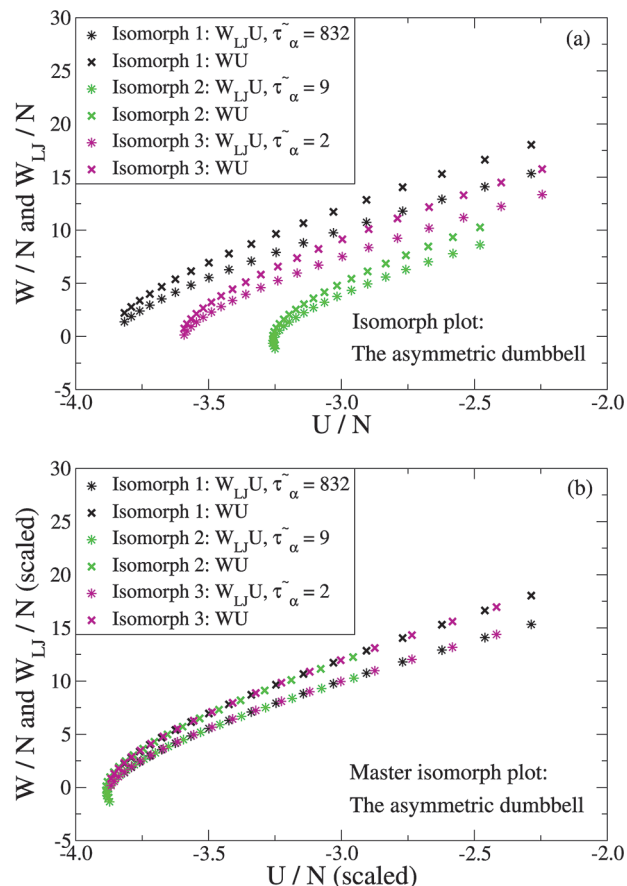


**Figure 23.** (a) Three different isomorphs for the asymmetric dumbbell model in two different versions with 19%, 21%, and 22% density increase, respectively (black, magenta, and green). The crosses give the total virial  $W$ , the asterisks give  $W_{\text{LJ}} = W - W_{\text{CON}}$ .  $\tilde{\tau}_\alpha$  is the reduced relaxation time of the isomorph extracted from the self-part of the intermediate scattering function. (b) The same isomorphs as in (a) where  $W_{\text{U}}$  and  $W_{\text{LJ}}/U$  are scaled to superpose with a factor identified by trial and error. The black points have unity scaling factor.

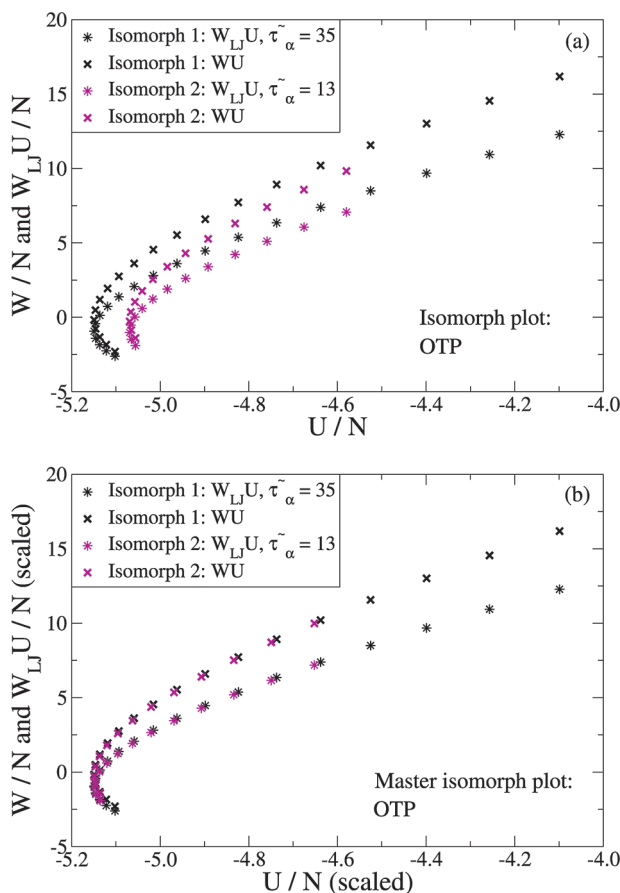


**Figure 24.** (a) Two different isomorphs for the OTP model in two different versions with 21% and 14% density increase (black and magenta). The crosses give the total virial  $W$ , the asterisks give  $W_{\text{LJ}} = W - W_{\text{CON}}$ .  $\tilde{\tau}_\alpha$  is the reduced relaxation time of the isomorph extracted from the self-part of the intermediate scattering function. (b) The same isomorphs as in (a) where  $W_{\text{U}}$  and  $W_{\text{LJ}} U$  are scaled to superpose with a factor identified by trial and error. The black points have unity scaling factor.

near straight line, the coefficients are not given by eqs 18 and 19. It is worth mentioning again that the prediction of ref 21 is for an atomic system and is as such not expected to hold for rigid molecular systems.

Finally, we consider in Figure 27 for the asymmetric dumbbell how the instantaneous fluctuations of  $W_{\text{CON}}$  correlate with  $W_{\text{LJ}}$  and  $W$ , respectively. The constraint contribution to the virial at this state point does not correlate well with the contribution to the virial coming from the LJ interactions ( $R = 0.31$ ). The correlation is higher when the total virial is considered ( $R = 0.61$ ). The main contribution to the virial for the asymmetric dumbbell model comes from the LJ interactions; however, the LJ virial does not correlate well with the constraint virial. The latter observation may indicate a breakdown of master isomorph scaling (for the total virial) at high pressures, but this remains to be confirmed.

## VI. SUMMARY AND OUTLOOK

Isomorphs are curves in the phase diagram of a strongly correlating liquid along which a number of static and dynamic quantities are invariant in reduced units. References 20 and 21 focused on understanding isomorphs in atomic systems. In this

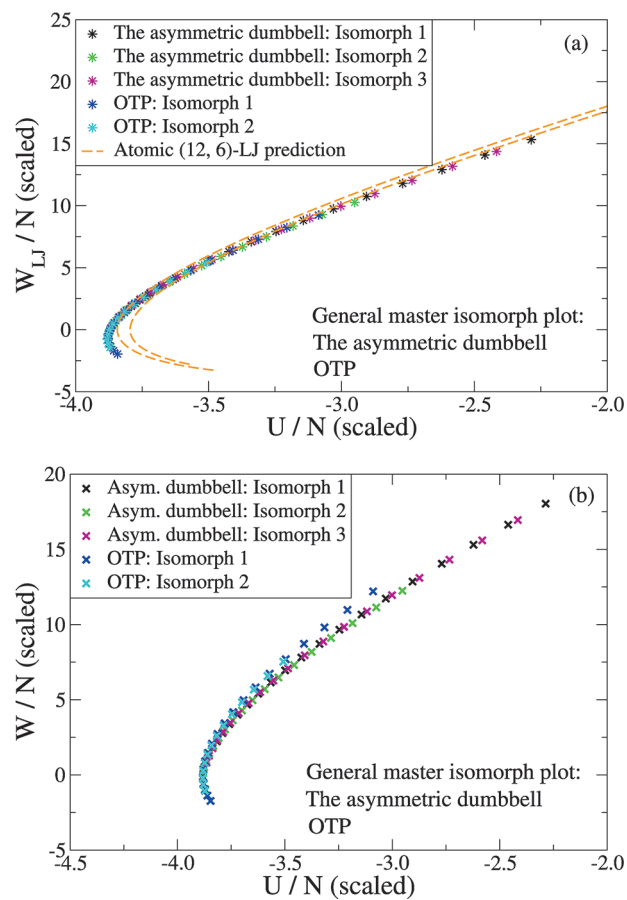


**Figure 25.** (a) Scaled  $W_{\text{LJ}} U$  isomorphs for the asymmetric dumbbell and OTP models. The black points have unity scaling factor. Both systems have intermolecular (12,6)-LJ interactions, and the dashed curves are the isomorph prediction from ref 21 for an atomic system, where the LJ reference coefficients have been calculated from the dumbbell state points  $(\rho, T) = (0.932, 0.465)$  and  $(0.851, 0.274)$ , respectively. (b) Scaled  $W_{\text{U}}$  isomorphs for the systems in (a). The total virial does not show exact scaling between the asymmetric dumbbell and OTP models.

paper we generalized the isomorph concept to deal with systems of rigid molecules (eq 5) and investigated several predicted isomorph invariants for the asymmetric dumbbell, a symmetric IPL dumbbell, and the Lewis–Wahnström OTP models. We find that these rigid molecular systems also have isomorphs to a good approximation; however, the isomorphs of the OTP model were more approximative than those of the asymmetric dumbbell, which is consistent with the OTP model being less strongly correlating. Moreover, it was found that the asymmetric dumbbell and Lewis–Wahnström OTP models to a good approximation have master isomorphs, i.e., that all isomorphs have the same shape in the virial/potential energy phase diagram. This applies for the total virial, but also after subtracting the constraint contribution. A general master isomorph was identified between these two model systems after this subtraction.

A full theoretical understanding of the implications of rigid bonds remains to be arrived at. For instance, the shape of molecular isomorphs is different from the shape of ref 21 for atomic LJ systems. The rigid bonds seem in general to increase  $\gamma$  and decrease the correlation coefficient  $R$  with respect to the unconstrained system. More specifically,  $R$

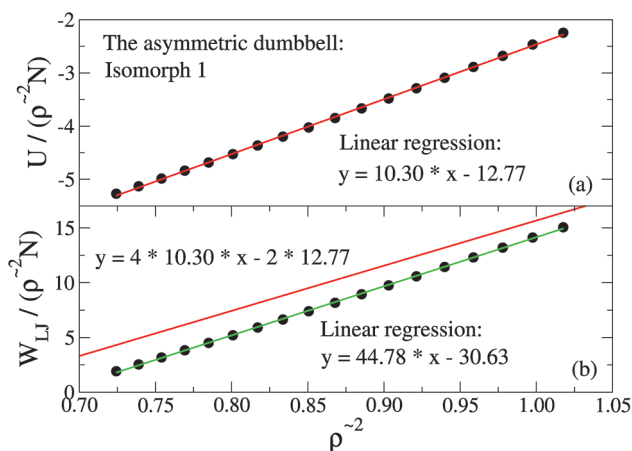


**Figure 26.** Potential energy and LJ virial as a function of  $\rho^2$  for “Isomorph 1” of the asymmetric dumbbell. (a) A linear regression fit of the potential energy has been performed to calculate the reference coefficients ( $U_m^*, U_n^*$ ). (b) These coefficients are then used to plot the red straight line, which according to the atomic prediction (eqs 18 and 19) should coincide with the black data points. The green line is a linear regression fit to the same data points.

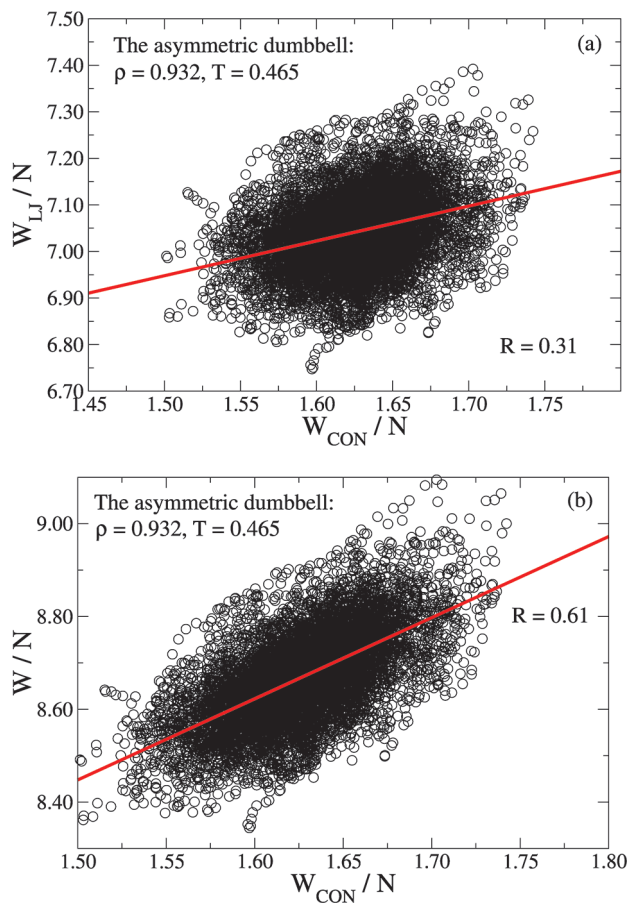


**Figure 27.** (a) Correlation of the instantaneous fluctuations of  $W_{LJ}$  and  $W_{CON}$ . The correlation coefficient  $R$  is 0.31. (b) Correlation of the instantaneous fluctuations of  $W$  and  $W_{CON}$ . The correlation coefficient  $R$  is 0.61.

decreases significantly with increasing asymmetric dumbbell bond length ( $R \approx 0.65$  around unity bond length; see section

IV'A). This is consistent with the results of Chopra et al.,<sup>10</sup> who noted a worse scaling of the reduced relaxation time and diffusion constant with excess entropy when the bond length of a rigid symmetric LJ dumbbell model is increased. On the other hand, it is noteworthy that strong correlation is observed for the OTP model even though it has unity bond lengths. The molecular center-of-mass structure in reduced units is predicted to be invariant along an isomorph; however, for the OTP model the reduced particle structure seems more invariant along an isomorph than the reduced molecular center-of-mass structure. The former is not predicted to be invariant along an isomorph, and the difference should be investigated in more detail to clarify this issue.

For real molecular liquids the concept of isomorphs is approximate. Thus it is natural to wonder to which extent the predicted scalings hold as the virial/potential energy correlation becomes worse. Consider for instance the supercooled regime. Here the transition states become increasingly more important as the temperature is lowered, and one might expect scalings involving dynamical quantities to be more sensitive to a decrease in the correlation coefficient than scalings based on the structure. Likewise, one could consider the breakdown of density scaling, indicated here by the study of the OTP model, as an effect of the correlation coefficient moving away from unity, because power-law density scaling is not solely based on Boltzmann factors. Quantifying how the scalings depend on the correlation coefficient is a topic that deserves more attention in future publications in connection with molecular liquids.

## ■ APPENDIX A: CONSTRAINED DYNAMICS AND THE VIRIAL EXPRESSION

Constrained dynamics is discussed in many different places, for instance refs 38, 40, and 41. We give here a brief introduction to constrained dynamics and the connection to the virial expression used in this article.

Gauss’ principle of least constraint<sup>48</sup> states that a classic mechanical system of  $N$  particles with constraints deviates instantaneously in a least possible sense from Newton’s second law, i.e., that

$$\sum_{i=1}^N m_i \left[ \ddot{\mathbf{r}}_i - \frac{\mathbf{F}_i}{m_i} \right]^2 \quad (A1)$$

is a minimum. Here  $\mathbf{r}_i$  and  $\mathbf{F}_i$  are the position and interaction force of particle  $i$ . In the case of no constraints, setting the partial derivative  $\partial/\partial\ddot{\mathbf{r}}_i$  to zero implies  $\ddot{\mathbf{r}}_i - \mathbf{F}_i/m_i = 0$ , i.e., Newton’s second law.

In the case of holonomic constraints  $\psi^\alpha(\mathbf{r}^N) = 0$  where  $\alpha = 1, \dots, G$ , the variation can be carried out by introducing Lagrangian multipliers, i.e.,

$$\sum_{i=1}^N m_i \left[ \ddot{\mathbf{r}}_i - \frac{\mathbf{F}_i}{m_i} \right]^2 - \sum_{\alpha=1}^G \lambda^\alpha \dot{\psi}^\alpha \quad (A2)$$

should be stationary. Setting the partial derivative  $\partial/\partial\ddot{\mathbf{r}}_i$  to zero implies (where a factor of 1/2 has been absorbed in the Lagrangian multiplier)

$$m_i \cdot \ddot{\mathbf{r}}_i = \mathbf{F}_i + \sum_{\alpha=1}^G \lambda^\alpha \nabla_{\mathbf{r}_i} \psi^\alpha = \mathbf{F}_i + \mathbf{G}_i \quad (A3)$$

Newton's second law thus remains valid if an additional force is added (called the constraint force  $\mathbf{G}_i$ ). At this point  $\lambda^\alpha$  is undetermined; however, an explicit expression<sup>40</sup> for  $\lambda^\alpha$  can be determined from differentiating twice with respect to time the holonomic constraint. In molecular dynamics simulations it is imperative to calculate  $\lambda^\alpha$  correctly to achieve a stable numerical algorithm. The reader is referred to refs 38 and 39 for details concerning this aspect.

The virial  $W$  is defined by  $W = 1/3\sum_{i=1}^N \mathbf{r}_i \cdot \mathbf{F}_i$ . In an atomic system with LJ pair potential interactions the virial is given by  $W = W_{\text{LJ}} = -1/3\sum_{i < j}^N r_{ij} u'(r_{ij})$ . If the system has bond constraints  $\psi^\alpha = (\mathbf{r}_{\alpha,i} - \mathbf{r}_{\alpha,j})^2/2 = r_{\alpha,ij}^2/2 = c_{\alpha,ij}^2/2$ , it follows from eq A3 that the constraint force contributes to the virial as  $W_{\text{CON}} = 1/3\sum_{i=1}^N \mathbf{r}_i \cdot \mathbf{G}_i = 1/3\sum_{\alpha=1}^G \lambda^\alpha r_{\alpha,ij}^2$ .

## ■ APPENDIX B: CONSTRAINED NVE AND NOSÉ–HOOVER NVT DYNAMICS IN REDUCED UNITS ALONG AN ISOMORPH

We start our considerations from the constrained equations of motion, eq A3:

$$m_i \cdot \ddot{\mathbf{r}}_i = \mathbf{F}_i + \sum_{\alpha=1}^G \lambda^\alpha \nabla_{\mathbf{r}_i} \psi^\alpha = \mathbf{F}_i + \mathbf{G}_i \quad (\text{B1})$$

Here  $\mathbf{r}_i$  and  $\mathbf{F}_i$  are, respectively, the position and interaction force of particle  $i$ , and  $\lambda^\alpha$  is the Lagrangian multiplier for the  $\alpha$ -th constraint  $\psi^\alpha$ . For simulating rigid molecules<sup>49</sup> the constraints are in general a combination of constrained bond lengths  $\psi^\alpha = (\mathbf{r}_{\alpha,i} - \mathbf{r}_{\alpha,j})^2/2 = r_{\alpha,ij}^2/2 = c_{\alpha,ij}^2/2$  and linear constraints  $\psi^\beta = \sum_{i=1}^{n_b} C_{\beta i} \mathbf{r}_i - \mathbf{r}_\beta = 0$ , where  $C_{\beta i}$  is a factor that depends on the geometry of the molecule (see ref 49 for more details). For simplicity we consider only bond constraints in the following.

The general expression for the Lagrangian multiplier  $\lambda^\alpha$  is given by<sup>40,50</sup>

$$\lambda^\alpha = - \sum_{\beta=1}^G (\mathbf{Z}^{-1})_{\alpha\beta} \left[ \sum_{i,j=1}^N \nabla_{\mathbf{r}_i} \nabla_{\mathbf{r}_j} \psi^\beta \dot{\mathbf{r}}_j \dot{\mathbf{r}}_i + \sum_{i=1}^N \frac{\nabla_{\mathbf{r}_i} \psi^\beta \cdot \mathbf{F}_i}{m_i} \right] \quad (\text{B2})$$

$$Z_{\alpha\beta} = \sum_{i=1}^N \frac{\nabla_{\mathbf{r}_i} \psi^\alpha \cdot \nabla_{\mathbf{r}_i} \psi^\beta}{m_i} \quad (\text{B3})$$

Defining reduced units for length, energy, and mass as follows

$$\tilde{\mathbf{r}}_i = \rho^{1/3} \mathbf{r}_i \quad (\text{B4})$$

$$\tilde{U} = U/k_B T \quad (\text{B5})$$

$$\tilde{m}_i = m_i / \langle m \rangle \quad (\text{B6})$$

reduced units for time and force follow as

$$\tilde{t} = t / (\rho^{-1/3} \sqrt{\langle m \rangle / k_B T}) \quad (\text{B7})$$

$$\tilde{\mathbf{F}}_i = \rho^{-1/3} \mathbf{F}_i / k_B T = - \nabla_{\tilde{\mathbf{r}}_i} \tilde{U} \quad (\text{B8})$$

Inserting the above definitions in eqs B1–B3 and using  $\nabla_{\mathbf{r}_i} \psi^\alpha = \mathbf{r}_{\alpha,ij}$  we arrive at the constrained NVE equations of motion in reduced units

$$\tilde{m}_i \cdot \ddot{\tilde{\mathbf{r}}}_i = \tilde{\mathbf{F}}_i + \sum_{\alpha=1}^G \tilde{\lambda}^\alpha \tilde{\mathbf{r}}_{\alpha,ij} = \tilde{\mathbf{F}}_i + \tilde{\mathbf{G}}_i \quad (\text{B9})$$

where

$$\tilde{\lambda}^\alpha = - \sum_{\beta=1}^G (\tilde{\mathbf{Z}}^{-1})_{\alpha\beta} \left[ \sum_{i,j=1}^N \dot{\tilde{\mathbf{r}}}_j \dot{\tilde{\mathbf{r}}}_i + \sum_{i=1}^N \frac{\tilde{\mathbf{r}}_{\beta,ij} \cdot \tilde{\mathbf{F}}_i}{\tilde{m}_i} \right] \quad (\text{B10})$$

$$\tilde{Z}_{\alpha\beta} = \sum_{i=1}^N \frac{\tilde{\mathbf{r}}_{\alpha,ij} \tilde{\mathbf{r}}_{\beta,ij}}{\tilde{m}_i} \quad (\text{B11})$$

Because, in general,  $\tilde{\mathbf{r}}_{\alpha,ij}^2 = \rho^{2/3} c_{\alpha,ij}^2$ , the reduced constrained equations of motion are *not* invariant along an isomorph.

Considering instead the molecular center-of-mass motion in reduced units

$$\tilde{M}_i \cdot \ddot{\tilde{\mathbf{r}}}_{\text{CM},i} = \tilde{\mathbf{F}}_{\text{CM},i} \quad (\text{B12})$$

where  $\tilde{\mathbf{F}}_{\text{CM},i}$  and  $\tilde{M}_i$  are respectively the reduced force on and mass of molecule  $i$ . Because the reduced force  $\tilde{\mathbf{F}}_{\text{CM},i}$  is invariant along an isomorph, it follows that the molecular NVE equations of motion are invariant along an isomorph. The invariance of  $\tilde{\mathbf{F}}_{\text{CM},i}$  can be seen as follows. The isomorph definition eq 5 implies for a fixed state point (1) and arbitrary state point ( $x$ ), both along the same isomorph [where  $\tilde{\mathbf{R}} \equiv (\rho^{-1/3} \tilde{\mathbf{r}}_{\text{CM},1}, \phi_1, \theta_1, \chi_1, \dots, \rho^{-1/3} \tilde{\mathbf{r}}_{\text{CM},N}, \phi_N, \theta_N, \chi_N)$ ], that

$$-U(\tilde{\mathbf{R}}^{(x)})/k_B T_x = -U(\tilde{\mathbf{R}}^{(1)})/k_B T_1 - \ln C_{1x} \quad (\text{B13})$$

Taking the gradient  $\nabla_{\tilde{\mathbf{r}}_{\text{CM},i}}$  it follows that

$$\tilde{\mathbf{F}}_{\text{CM},i}^{(x)} = \tilde{\mathbf{F}}_{\text{CM},i}^{(1)} \quad (\text{B14})$$

This concludes the proof of the isomorph invariance of the reduced molecular center-of-mass NVE equations of motion. For the molecular center-of-mass NVT equations of motion the proof is analogous to the above and shown for atomic systems in ref 20. In this case the time constant of the Nosé–Hoover algorithm needs to be adjusted along the isomorph; otherwise, the dynamics is not invariant.<sup>20</sup>

## ■ ACKNOWLEDGMENT

The Centre for Viscous Liquid Dynamics “Glass and Time” is sponsored by the Danish National Research Foundation (DNRF).

## ■ REFERENCES

- Alba-Simionescu, C.; Cailliaux, A.; Alegria, A.; Tarjus, G. *Europhys. Lett.* **2004**, *68*, S8.
- Dreyfus, C.; Grand, A. L.; Gapinski, J.; Steffen, W.; Patkowski, A. *Eur. Phys. J. B* **2004**, *42*, 309.
- Roland, C. M. *Macromolecules* **2010**, *43*, 7875.
- Roland, C. M.; Casalini, R.; Paluch, M. *Chem. Phys. Lett.* **2003**, *367*, 259.
- Ngai, K. L.; Casalini, R.; Capaccioli, S.; Paluch, M.; Roland, C. M. *J. Phys. Chem. B* **2005**, *109*, 17356.
- Rosenfeld, Y. *Phys. Rev. A* **1977**, *15*, 2545.
- Rosenfeld, Y. *J. Phys.: Condens. Matter* **1999**, *11*, 5415.
- Chopra, R.; Truskett, T. M.; Errington, J. R. *J. Phys. Chem. B* **2010**, *114*, 10558.
- Chopra, R.; Truskett, T. M.; Errington, J. R. *J. Phys. Chem. B* **2010**, *114*, 16487.
- Chopra, R.; Truskett, T. M.; Errington, J. R. *J. Chem. Phys.* **2010**, *133*, 104506.
- Abramson, E. H. *Phys. Rev. E* **2007**, *76*, 051203.
- Abramson, E. H.; West-Foyle, H. *Phys. Rev. E* **2008**, *77*, 041202.
- Abramson, E. H. *Phys. Rev. E* **2009**, *80*, 021201.

- (14) Galliero, G.; Boned, C.; Fernández, J. *J. Chem. Phys.* **2011**, *134*, 064505.
- (15) Fragiadakis, D.; Roland, C. M. *J. Chem. Phys.* **2011**, *134*, 044504.
- (16) López, E. R.; Pensado, A. S.; Comuñas, M. J. P.; Pádua, A. A. H.; Fernández, J.; Harris, K. R. *J. Phys. Chem.* **2011**, *134*, 144507.
- (17) Bailey, N. P.; Pedersen, U. R.; Gnan, N.; Schröder, T. B.; Dyre, J. C. *J. Chem. Phys.* **2008**, *129*, 184507.
- (18) Bailey, N. P.; Pedersen, U. R.; Gnan, N.; Schröder, T. B.; Dyre, J. C. *J. Chem. Phys.* **2008**, *129*, 184508.
- (19) Schröder, T. B.; Bailey, N. P.; Pedersen, U. R.; Gnan, N.; Dyre, J. C. *J. Chem. Phys.* **2009**, *131*, 234503.
- (20) Gnan, N.; Schröder, T. B.; Pedersen, U. R.; Bailey, N. P.; Dyre, J. C. *J. Chem. Phys.* **2009**, *131*, 234504.
- (21) Schröder, T. B.; Gnan, N.; Pedersen, U. R.; Bailey, N. P.; Dyre, J. C. *J. Chem. Phys.* **2011**, *134*, 164505.
- (22) Schröder, T. B.; Pedersen, U. R.; Bailey, N. P.; Toxvaerd, S.; Dyre, J. C. *Phys. Rev. E* **2009**, *80*, 041502.
- (23) Pedersen, U. R.; Gnan, N.; Bailey, N. P.; Schröder, T. B.; Dyre, J. C. *J. Non-Cryst. Solids* **2011**, *357*, 320.
- (24) Pedersen, U. R.; Bailey, N. P.; Schröder, T. B.; Dyre, J. C. *Phys. Rev. Lett.* **2008**, *100*, 015701.
- (25) Coslovich, D.; Roland, C. M. *J. Chem. Phys.* **2009**, *130*, 014508.
- (26) Coslovich, D.; Roland, C. M. *J. Phys. Chem. B* **2008**, *112*, 1329.
- (27) Kob, W.; Andersen, H. C. *Phys. Rev. E* **1995**, *51*, 4626.
- (28) Kob, W.; Andersen, H. C. *Phys. Rev. E* **1995**, *52*, 4134.
- (29) Wahnström, G.; Lewis, L. J. *Physica A* **1993**, *201*, 150.
- (30) Lewis, L. J.; Wahnström, G. *Phys. Rev. E* **1994**, *50*, 3865.
- (31) Gundermann, D.; Pedersen, U. R.; Hecksher, T.; Bailey, N. P.; Jakobsen, B.; Christensen, T.; Olsen, N. B.; Schröder, T. B.; Fragiadakis, D.; Casalini, R.; Roland, C. M.; Dyre, J. C.; Niss, K. *Nat. Phys.* **2011**, *7*, 816.
- (32) In practice, it is only required that the physically relevant configurations obey this scaling, i.e., at least those that contribute significantly to the partition function.
- (33) Gray, C. G.; Gubbins, K. E. *Theory of Molecular Fluids*; Oxford University Press: Oxford, U.K., 1984.
- (34) Lazaridis, T.; Paulaitis, M. E. *J. Phys. Chem.* **1992**, *96*, 3847.
- (35) Lazaridis, T.; Karplus, M. *J. Chem. Phys.* **1996**, *105*, 4294.
- (36) Pedersen, U. R.; Hudson, T. S.; Harrowell, P. *J. Chem. Phys.* **2011**, *134*, 114501.
- (37) Hess, B.; Kutzner, C.; van der Spoel, D.; Lindahl, E. *J. Chem. Theory Comput.* **2008**, *4*, 435.
- (38) Toxvaerd, S.; Heilmann, O. J.; Ingebrigtsen, T.; Schröder, T. B.; Dyre, J. C. *J. Chem. Phys.* **2009**, *131*, 064102.
- (39) Ingebrigtsen, T.; Heilmann, O. J.; Toxvaerd, S.; Dyre, J. C. *J. Chem. Phys.* **2010**, *132*, 154106.
- (40) Edberg, R.; Evans, D. J.; Morriss, G. P. *J. Chem. Phys.* **1986**, *84*, 6933.
- (41) Ryckaert, J. P.; Ciccotti, G.; Berendsen, H. J. C. *J. Comput. Phys.* **1977**, *23*, 327.
- (42) Nosé, S. *J. Chem. Phys.* **1984**, *81*, 511.
- (43) Hoover, W. G. *Phys. Rev. A* **1985**, *31*, 1695.
- (44) Toxvaerd, S. *Mol. Phys.* **1991**, *72*, 159.
- (45) All simulations were performed using a molecular dynamics code optimized for NVIDIA graphics cards, which is available as open source code at <http://rumd.org>.
- (46) Frenkel, D.; Smit, B. *Understanding Molecular Simulation*; Academic Press: New York, 2002.
- (47) Pedersen, U. R.; Schröder, T. B.; Dyre, J. C. *Phys. Rev. Lett.* **2010**, *105*, 157801.
- (48) Gauss, K. F. *J. Reine Angew. Math.* **1829**, *4*, 232.
- (49) Ciccotti, G.; Ferrario, M.; Ryckaert, J. P. *Mol. Phys.* **1982**, *47*, 1253.
- (50) Melchionna, S. *Phys. Rev. E* **2000**, *61*, 6165.